NASA Technical Memorandum 110171

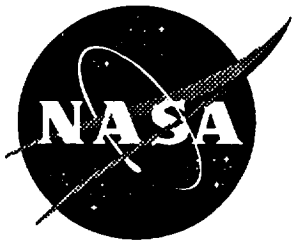

Global and Local Stress Analyses of McDonnell Douglas Stitched/RFI Composite Wing Stub Box

John T. Wang
Langley Research Center, Hampton, Virginia

March 1996

National Aeronautics and
Space Administration
Langley Research Center
Hampton, Virginia 23681-0001

Global and Local Stress Analyses of McDonnell Douglas Stitched/RFI Composite Wing Stub Box

John T. Wang
NASA Langley Research Center
Hampton, Virginia

Abstract

This report presents the results of a pretest structural analysis of an all-composite stitched/RFI (resin film infusion) wing stub box which was designed and fabricated by the McDonnell Douglas Aerospace Company. Geometrically nonlinear structural responses of the wing stub box were predicted by using the finite element analyses and a global/local approach in which the global model contains the entire test article while the local model contains a large nonlinearly deformed region in the upper cover of the wing stub box. The wing box test article includes the all-composite wing stub box, a metallic load-transition box and a metallic wing-tip extension box. The two metallic boxes were connected to the inboard and outboard ends of the composite wing stub box, respectively. The metallic load-transition box was attached to a steel and concrete vertical reaction structure. In the global analysis, an upward load was applied at the tip of the extension box to induce bending of the wing stub. Global analysis found that an upper cover region, which contains three stringer runouts, exhibits large nonlinear deformations. Hence, a local model refined in the nonlinearly deformed region was created to predict more accurate strain results near stringer runouts. Numerous global and local analysis results such as deformed shapes, displacements at selected locations, and strains at critical locations are included in this report.

Introduction

The purpose of this report is to document the pretest structural analysis results for an advanced stitched/RFI (resin film infusion) graphite/epoxy wing stub box. This advanced stitched/RFI graphite/epoxy wing stub box, representing the inboard portion of a civil-transport-aircraft high-aspect-ratio wing stub box, was designed and manufactured by McDonnell Douglas Aerospace (MDA) Company under the support of NASA's Advanced Composites Technology (ACT) Program. The innovative stitched/RFI process used to fabricate this all-composite wing stub box has the potential for reducing manufacturing costs while producing damage tolerant composite aircraft primary structures.

A preliminary global analysis was performed by McDonnell Douglas engineers[1]. More refined nonlinear analyses of the global model and a local model were performed by NASA Langley Research Center engineers to support the structural wing-stub-box tests at NASA Langley. The global model contains the entire test article which includes an all-composite stub box, an inboard metallic load transition box and an outboard metallic wing-tip extension box. The local model contains an upper cover region surrounding the location of three stringer runouts (where a stiffener terminates at a rib). It was found that this region exhibits large nonlinear deformations. Hence, a more refined mesh was used in the local model to obtain more accurate stress analysis results. Displacements obtained by the global model analysis were applied to the boundaries of the local model. Deformed shapes, displacements at selected locations, and strains in critical regions generated from the global and local analyses were used for instrumenting the wing stub box. Only the analysis results are presented in this report. These analytical results have been correlated with test results and the correlation will be presented in another paper [2].

Wing Stub Box Test Article

A photograph of the wing stub box test article is shown in Figure 1 and the dimensions of the wing stub box are provided in Figure 2. The composite wing stub box is about 12 ft long and 8 ft wide, and its maximum depth at the root is about 2.3 ft. The wing stub box test article includes the all-composite stub box, the inboard transition box (made of steel and aluminum), and the outboard extension box (made of steel). The all-composite stub box weighs approximately 1200 lbs while the entire wing stub box test article weighs about 7600 lbs. In its test configuration, the transition box was attached to a steel and concrete strongback (test wall) at the NASA Langley Structural Mechanics Test Laboratory. The extension box is a load introduction structure and the ultimate design load, a vertical load at the tip of the extension-box front spar, is 166,000 lbs.

The upper-cover-panel construction of the all-composite wing stub box shown in Figure 3 contains a skin panel, ten blade stiffeners, five ribs, two metal angles, two spar caps, and has a 22.5 in. by 12.5 in. oval access door cutout. The upper cover skin, flanges, and blade stiffeners were constructed from AS4/3501-6 graphite/epoxy composite with repeating sublaminates (stacks). The layup sequence of a stack is [45/-45/0/90/0/-45/45] and the nominal total thickness of a stack after curing is 0.058 in. The upper skin thickness varies from five stacks (0.29 in.) to ten stacks (0.58 in.) as shown in Figure 4. All the blade stiffeners of the upper cover

have the same thickness and each has eight stacks (0.464 in.). The upper-cover panel was fabricated by first assembling and stitching all the dry preform components together and then using a resin film infusion process to infuse resin into the preform. Each dry preform component such as the skin or the stiffener was stitched individually before assembling the upper-cover-panel. The stiffener flanges are stitched to the skin so that no mechanical fasteners are required. This reduces the manufacturing costs. However, at the stiffener runout locations, fasteners were installed after the RFI process to prevent skin stiffener debonding at these locations. Moreover, the access door cutout was reinforced by a composite land ring which was bolted to the panel skin using 0.3125 inch diameter bolts. To further examine the region between Ribs 6 and 8, which contains three stringer runouts and two metal angles as shown in Figure 3, a local refined nonlinear analysis was carried out.

The interior of the wing stub box is shown in Figure 5 in which the five ribs and the two spar webs are made of conventional AS4/3501-6 prepreg material. The spar webs have a constant thickness of 0.31 in. and the rib webs have a constant thickness of 0.15 in. Moreover, the ribs and spars are stiffened with composite stiffeners to prevent buckling. The lower skin is made of stitched/RFI graphite/epoxy material with IM7 fibers in the 0-degree fiber direction and AS4 fibers in all the other fiber directions. The thickness of the lower skin, (which is thicker than the upper skin), ranges from .33 in. to .82 in. The high moduli of IM7 fibers and thicker skin result in smaller strains for the lower skin; therefore no failure is expected in the lower skin region and the results in this report relate mainly to the upper cover panel.

Material Properties and Allowables

The equivalent AS4/3501-6 material properties for the upper skin panel laminates used in the analyses are

$$E_x = 8.17\ Msi$$
$$E_y = 4.46\ Msi$$
$$G_{xy} = 2.35\ Msi$$
$$\nu_{xy} = 0.459$$

and the equivalent AS4/IM7/3501-6 material properties for the lower skin panel laminates used in the analyses are

$$E_x = 11.85\ Msi$$
$$E_y = 4.55\ Msi$$
$$G_{xy} = 2.57\ Msi$$
$$\nu_{xy} = 0.409$$

Note that the x-direction, which is parallel to the rear spar, is coincident with the 0-degree fiber direction and the y-direction is coincident with the 90-degree fiber direction. The ultimate compression strain allowable in the x-direction of the undamaged upper skin laminate is $9330\,\mu\varepsilon$ and the 0.3125 inch diameter filled hole B-base compression strain allowable is $8100\,\mu\varepsilon$ [1].

Global and Local Finite Element Models

The global finite element model shown in Figure 6 was used to determine the global responses of the complete test article and this global model contains 4408 quadrilateral elements (CQUAD4), 99 triangular elements (CTRIA3), 1308 beam elements (CBEAM), 798 rod elements (CONROD) and 742 rigid bar elements (RBAR). The finite element analyses were performed using MSC/NASTRAN [3], V68. The upper skin, lower skin, rib webs and spar webs were modeled as plate elements (CQUAD4 and CTRIA3), and the stiffeners were modeled as beam elements (CBEAM). A total of 5,266 grid points were used in the global model.

A finer finite element mesh was used around the access door cutout to better define the high stress concentration in that region. Grid points of each composite stiffener were positioned along its centroidal axis. Therefore, the stiffener elements, modeled as beam elements, were offset from the skin. These stiffener beam elements were rigidly connected to the skin by relatively stiff CBEAM elements. The finite element mesh of the wing stub box interior region is shown in Figure 7 in which all the rib webs including cutout holes were modeled. Both buckling analysis and geometrically nonlinear analysis of the global model were performed by using MSC/NASTRAN and the solution sequences used for buckling analysis and nonlinear static analysis were SOL 105 and SOL 106, respectively.

As mentioned earlier, the local finite element model contains an upper cover region surrounding three stringer runouts as shown in Figure 8. The location of the local model on the stub box is clearly shown in Figure 9 in which the local model is superposed on the global model. Structural details near a typical stiffener runout region are shown in Figure

10. Note that the tapering of the blade stiffener flange and the blade web in the runout region and a small gap existing between the stiffener flange and rib flange were also modeled in the local model. The blade stiffener web is attached to the rib web, but it is not connected to the rib flange. The local finite element model shown in Figure 8 has 2642 quadrilateral shell elements, 8 triangular elements and 2738 nodes. Displacement boundary conditions of the local model were obtained through spline interpolation of the global displacement results. NASA Langley's COMET (Computational Mechanics Testbed) finite element code [4] was used for the nonlinear analysis of this local model.

The global model was originally created by engineers at the McDonnell Douglas Aerospace Company and some modifications were performed by engineers at NASA Langley. PATRAN [5] was used to modify the global model and was also used to create the local model. Results from both the global and local analyses were postprocessed using PATRAN.

Analysis Results

Global analysis results

A buckling analysis of the wing-stub-box global model was performed first and the critical buckling load was found to be 11.2 % higher than the ultimate design load of 166,000 lbs with the buckling mode shape shown in Figure 11. The second analysis performed was a geometrically nonlinear NASTRAN analysis and the predicted deformed shape of the whole test article at ultimate load is shown in Figure 12. The jack loading displacements predicted at ultimate load were u= -0.2169 in, v=0.1629 in, and w=13.4887 in. The predicted relationship between the load and the vertical displacement at the loading point is approximately linear as shown in Figure 13. The close-up view of the deformed shape of the composite wing stub box is shown in Figure 14. Note that the wavy deformation of the upper skin is likely caused by a lack of longitudinal stiffener support near the access door cutout and its two adjacent outboard bays as shown in Figure 3. Figure 15 illustrates the out-of-plane (z-direction) deflections in the deformed region along two lines, labeled A-A and B-B, parallel to the major axis of the elliptic cutout. Line B-B, located at 15.875 in. from Line A-A, is in location which sees less wavy deformation and the difference of the out-of-plane displacements between these two lines provides a good measurement of the nonlinearity developing in the two bays outboard of the access door.

The predicted out-of-plane displacements at six LVDT (Linear Voltage Displacement Transducer) locations on the lower skin are plotted in Figure 16. Locations 1 to 3 are on the rear spar while Locations 4 to 6 are on the front spar (see insert in Figure 16 and the Douglas Aircraft Company Tasks Assignment Drawings TAD Z7944503). All the out-of-plane displacements are seen to be linearly related to the applied load.

All the strain results presented for the global model are based on the NASTRAN element coordinate system. The element x-axis is coincident with the global x-axis except in the access door cutout region where the element x-axis is tangent to the edge of the cutout (in the circumferential direction). Strain contour plots (ε_{xx}) of the upper composite skin panel are plotted in Figures 17-19. High strains occur at the edge of the access door cutout. Close-up strain contour plots for the skin side, mid-surface and stiffener side of the upper cover in the cutout region are in Figures 20 to 22. High strains are predicted in the circumferential direction of the cutout: $9100\mu\varepsilon$ at the skin side, $6650\mu\varepsilon$ at the stiffener side, and $6770\mu\varepsilon$ at the midsurface.

Predicted strains at all strain gage locations for 100% and 50% of the ultimate load are listed in Tables I to IV in which the strain gage locations and the completed term of every abbreviation can be found in Douglas Aircraft Company Tasks Assignment Drawings TAD Z7944503. Note that the strain gage patterns for the upper and lower skins are shown in Figures 23 and 24.

Strain versus load plots are generated for some strain gages located in high strain regions including these gages near the access door cutout (gages 78, 79, and 612) and in the highly nonlinear deformed regions (gages 63, 64, 67, and 68). Locations of these gages are shown in Figure 25 and predicted strain versus load plots at these gage locations can be found in Figures 26 to 30.

Local analysis results

A geometrically nonlinear analysis was performed with the local model using the COMET code and the displacement boundary conditions obtained from the nonlinear global analyses. These displacement boundary conditions were applied on the four edges of the local model and the root of the middle rib. The predicted deformed shape of the local model at the ultimate loading condition is shown in Figure 31. Note that the skin is deformed to the stiffener side which may be due to the lack of longitudinal

stiffener support in one of the skin bays. The skin strain contour plots at the ultimate load, as derived from the nonlinear analysis, are plotted in Figures 32 to 34 at the skin side, stiffener side, and mid-surface. The strains in the skin side are much higher than in the stiffener side due to the significant skin bending deformation shown in Figure 31.

Figures 35 to 37 display the variation of the strain in the x-direction with load for the three gaps between the stiffener flange and rib flange, (see Figure 10), located at the stiffener runouts, (labeled #1 to #3 in Figure 8), for the skin side, mid-surface, and stiffener side locations. Predicted lateral strains (in y-direction) in the rib webs are plotted in Figures 38-40. Significant rib-web bending was predicted at the runouts where the stiffener webs attach to the ribs.

Predicted strains at all strain gage locations in the local model region for 100% and 50% of the ultimate load are listed in Tables V and VI. Note that the strain gage locations can be found from Figure 23.

The existence of the stiffener runouts and the large skin bending deformations may induce the stiffener-skin separation loads, defined as the vertical or normal stress resultants between the blade and the skin. The blade stiffeners in the local model are numbered from 1 to 4 as shown in Figure 8. The separation load of the front spar may not be an issue because the front spar cap is mechanically fastened to the skin, thus only the separation load results for blade stiffeners are presented and plotted in Figures 41 to 44. The horizontal axes of these plots are the distance measured from an edge of the local model in the positive x-direction (see insert of each plot). These results can be compared with blade stiffener separation allowables [6]. The ultimate failure load of blade stiffener separation tests performed in Reference 6 is about 2500 lbs/in which is much higher than the predicted separation loads here. Therefore, no stiffener-skin separation failure is expected.

Concluding Remarks

This report documents the global and local geometrically nonlinear finite element analysis results, generated by engineers at NASA Langley, of the McDonnell Douglas Stitched/RFI wing stub box. These analyses were performed by the Computational Structures Branch of NASA Langley Research Center. Results have been used for strength prediction of the stub box and determination of the instrumentation and gage locations of the stub box test article. When the actual structural tests are performed on the stub box, analysis results will be correlated with the test data.

Acknowledgment

The author wishes to acknowledge the analytical support provided by Thiagaraja Krishnamurthy, Brian Mason and Tina Lotts of Analytical Services and Materials Inc.

References

1. Hinrichs, S. C., "ICAPS Stub Box Structural Analysis," Vols. I to VII., MDC94K9101, Preliminary, Feb. 6, 1995

2. Wang, J. T., Jegley, D. C., Bush, H. G., and Hinrichs, S. C., "Correlation of Structural Analysis and Test Results for the McDonnell Douglas Stitched/RFI All Composite Wing Stub Box," to be presented in the 11th DoD/NASA/FAA Conference on Fibrous Composites in Structural Design, Fort Worth, TX, Aug. 26-29, 1996.

3. Anon., MSC/NASTRAN Reference Manual, Version 68, The MacNeal-Schwendler Corporation, April. 1994.

4. "The Computational Structural Mechanics Testbed User's Manual," NASA TM-100644, Oct. 1989.

5. Anon., PATRAN Plus User Manual, Release 2.4, PDA Engineering, Publication Number 2191023, Sept. 1989.

6. Hinrichs, S. C., "Stitched Stringer Tension Pull-Off Subcomponent Test Report," MDC94K9103, Jan. 5, 1995.

Table I. Strain prediction from global model at ultimate load of 166,000 lbs (including all gages on external upper skin).

Strain Gage No	Angle	Surface	Location	Micro Strain	Node Number in FEM Model
2	0.0	ext	Upr.Skin	-3465.4	196
4	0.0	ext	Upr.Skin	-3758.9	194
5	0.0	ext	Upr.Skin	-5032.7	65
6	45.0	ext	Upr.Skin	-1761.4	65
7	90.0	ext	Upr.Skin	1821.7	65
11	0.0	ext	Upr.Skin	-4978.8	1359
12	0.0	ext	Upr.Skin	-4978.8	1359
15	0.0	ext	Upr.Skin	-4556.0	614
16	0.0	ext	Upr.Skin	-4556.0	614
17	0.0	ext	Upr.Skin	-4224.8	71
18	0.0	ext	Upr.Skin	-4842.3	414
20	0.0	ext	Upr.Skin	-4953.4	437
22	0.0	ext	Upr.Skin	-5194.9	371
25	0.0	ext	Upr.Skin	-4210.0	101
26	0.0	ext	Upr.Skin	-4433.7	403
27	45.0	ext	Upr.Skin	-805.2	403
28	90.0	ext	Upr.Skin	1395.3	403
32	0.0	ext	Upr.Skin	-4085.5	401
37	0.0	ext	Upr.Skin	-4750.7	474
39	0.0	ext	Upr.Skin	-4609.1	523
46	0.0	ext	Upr.Skin	-4924.3	885
46	0.0	ext	Upr.Skin	-4924.3	885
48	-13.0	ext	Upr.Skin	-4522.1	47

Table I (Continued)

Strain prediction from global model at ultimate load of 166,000 lbs.

Strain Gage No	Angle	Surface	Location	Micro Strain	Node Number in FEM Model
50	0.0	ext	Upr.Skin	-4465.8	518
51	0.0	ext	Upr.Skin	-4430.3	877
52	45.0	ext	Upr.Skin	-543.4	877
53	90.0	ext	Upr.Skin	1679.8	877
58	0.0	ext	Upr.Skin	-3050.7	125
62	0.0	ext	Upr.Skin	-3581.4	872
63	0.0	ext	Upr.Skin	-4809.6	1328
67	0.0	ext	Upr.Skin	-1910.8	121
65	0.0	ext	Upr.Skin	-4257.0	864
67	0.0	ext	Upr.Skin	-1910.8	121
69	0.0	int	Int.Coast	1201.7	Q3098/99
70	45	int	Int.Coast	535.5	Q3098/99
71	90	int	Int.Coast	-681.0	Q3098/99
72	0.0	ext	Upr.Skin	-3473.1	68
74	-13.0	ext	Upr.Skin	-2434.0	107
75	0.0	ext	Upr.Skin	-6015.1	117
77	-13.0	ext	Upr.Skin	-1324.6	221
78	0.0	ext	Upr.Skin	-8430.2	43
79	0.0	ext	Upr.Skin	-7868.0	25
81	0.0	ext	Upr.Skin	-6647.8	62
84	0.0	ext	Upr.Skin	-5017.2	63
92	0.0	ext	Upr.Skin	-5082.1	1234
93	0.0	ext	Upr.Skin	-5485.3	1292
94	0.0	ext	Upr.Skin	-2647.8	614
95	0.0	ext	Upr.Skin	-2647.8	614
96	0.0	ext	Upr.Skin	-4978.8	1359
97	0.0	ext	Upr.Skin	-4978.8	1359

Table I (Continued)

Strain prediction from global model at ultimate load of 166,000 lbs.

Strain Gage No	Angle	Surface	Location	Micro Strain	Node Number in FEM Model
102	0.0	int	Lwr.Skin	2231.2	1467
123	0.0	int	Lwr.Skin	1957.8	2244
125	0.0	int	Lwr.Skin	2475.8	2260
128	0.0	int	Lwr.Skin	2616.2	2276
136	0.0	int	Lwr.Skin	2493.4	1371
140	0.0	int	Lwr.Skin	3138.0	1452
144	0.0	ext	Lwr.Skin	3184.9	1605
201	-45.0	aft	Fwd.spar	-280.4	3007
205	-45.0	aft	Fwd.spar	-139.7	2955
209	-45.0	aft	Fwd.spar	-664.6	2891
302	0.0	aft	Rear.Spar	-1102.3	3324
303	45.0	aft	Rear.Spar	27.0	3324
304	90.0	aft	Rear.Spar	352.9	3324
306	0.0	aft	Rear.Spar	-779.5	3307
307	45.0	aft	Rear.Spar	136.2	3307
308	90.0	aft	Rear.Spar	348.4	3307
310	0.0	aft	Rear.Spar	-194.1	3292
311	45.0	aft	Rear.Spar	1044.3	3292
312	90.0	aft	Rear.Spar	-383.5	3292
444	45.0	inb	RIB.4	-380.3	3703
445	90.0	inb	RIB.4	-114.1	3651
448	0.0	inb	RIB.4	986.5	3674
454	45.0	inb	RIB.5	530.0	3918
455	90.0	inb	RIB.5	56.2	3823
464	-45.0	inb	Rib.6	168.7	3960
465	90.0	inb	Rib.6	50.6	3961

Table I (Continued)

Strain prediction from global model at ultimate load of 166,000 lbs.

Strain Gage No	Angle	Surface	Location	Micro Strain	Node Number in FEM Model
468	0.0	inb	Rib.6	-318.3	4167
474	-45.0	inb	Rib.7	-173.0	4348
475	90.0	inb	Rib.7	92.6	4173
478	0.0	inb	Rib.7	-195.7	4250
484	-45.0	inb	Rib.8	-180.8	4475
485	90.0	inb	Rib.8	82.1	4382
488	0.0	inb	Rib.8	549.8	4507
501	0.0	fwd	Ext.Box	138.6	5104
502	-45.0	fwd	Ext.Box	-2483.7	5104
503	90.0	fwd	Ext.Box	-316.5	5104
507	0.0	int	Ext.Box	282	Q4160
511	0.0	ext	Tr.Str.Up	55.1	4852
513	0.0	ext	Tr.Str.Up	47.3	4865
602	0.0	ext	Upr.Skin	-4670.7	387
604	0.0	ext	Upr.Skin	-4924.9	421
606	0.0	ext	Upr.Skin	-5083.4	453
610	-13.0	ext	Upr.Skin	-1618.8	221
611	0.0	ext	Upr.Skin	-3885.6	49
612	0.0	ext	Upr.Skin	-8596.0	39
613	0.0	ext	Upr.Skin	-2281.1	120
614	0.0	ext	Upr.skin	-2489.0	69
615	0.0	ext	Upr.skin	-4350.3	444
616	0.0	ext	Upr.skin	-4551.4	449
617	0.0	ext	Upr.skin	-4924.3	885

Table II. Strain prediction from global model at ultimate load of 166,000 lbs (including all gages on internal upper skin).

Strain Gage No	Angle	Surface	Location	Micro Strain	Node Number in FEM Model
1	0.0	int	Upr.Skin	-4015.2	196
3	0.0	int	Upr.Skin	-4488.6	194
9	0.0	int	Upr.Skin	-4780.7	1359
10	0.0	int	Upr.Skin	-4780.7	1359
13	0.0	int	Upr.Skin	-4389.4	614
14	0.0	int	Upr.Skin	-4389.4	614
30	90.0	int	Upr.Skin	1607.8	399
31	0.0	int	Upr.Skin	-4032.7	401
33	0.0	int	Upr.Skin	400.9	4336
34	45.0	int	Upr.Skin	520.7	4336
35	90.0	int	Upr.Skin	708.9	4336
36	0.0	int	Upr.Skin	-4242.4	474
38	0.0	int	Upr.Skin	-4326.3	523
40	0.0	int	Upr.Skin	500.4	4388
41	45.0	int	Upr.Skin	279.8	4388
42	90.0	int	Upr.Skin	595.0	4388
43	0.0	int	Upr.Skin	-4986.1	885
44	0.0	int	Upr.Skin	-2526.6	885
47	-103.0	int	Upr.Skin	1627.0	493
64	0.0	int	Upr.Skin	-2639.8	1328
68	0.0	int	Upr.Skin	-3500.6	121
80	0.0	int	Upr.Skin	-5589.5	25
87	0.0	int	Upr.Skin	-5071.2	1292
91	0.0	int	Upr.Skin	-5176.1	1234
101	0.0	ext	Lwr.Skin	2582.9	1496
103	0.0	ext	Lwr.Skin	2803.8	1550
104	45.0	ext	Lwr.Skin	496.4	1550
105	90.0	ext	Lwr.Skin	-1096.2	1550

Table II (Continued)

Strain prediction from global model at ultimate load of 166,000 lbs.

Strain Gage No	Angle	Surface	Location	Micro Strain	Node Number in FEM Model
107	0.0	ext	Lwr.Skin	2640.0	1667
109	0.0	ext	Lwr.Skin	3342.7	1558
111	0.0	ext	Lwr.Skin	2898.7	1574
112	45.0	ext	Lwr.Skin	975.5	1574
113	90.0	ext	Lwr.Skin	-1076.0	1574
115	0.0	ext	Lwr.Skin	3001.5	1446
116	0.0	ext	Lwr.Skin	2535.1	1691
118	0.0	ext	Lwr.Skin	2296.7	1784
119	45.0	ext	Lwr.Skin	570.7	1784
120	90.0	ext	Lwr.Skin	-706.9	1784
122	13.0	ext	Lwr.Skin	794.6	1385
124	13.0	ext	Lwr.Skin	2099.3	1374
126	0.0	ext	Lwr.Skin	2354.4	2273
129	0.0	ext	Lwr.Skin	2627.3	2287
131	0.0	ext	Lwr.Skin	2620.1	1808
132	45.0	ext	Lwr.Skin	405.3	1808
133	90.0	ext	Lwr.Skin	-843.0	1808
137	13.0	ext	Lwr.Skin	3169.2	1371
138	0.0	ext	Lwr.Skin	2936.5	2276
139	0.0	ext	Lwr.Skin	3050.8	2291
202	0.0	fwd	Fwd.spar	-673.2	3007
203	-45.0	fwd	Fwd.spar	-370.2	3007
204	90.0	fwd	Fwd.spar	-574.1	2007
206	0.0	fwd	Fwd.spar	-541.3	2955
207	-45.0	fwd	Fwd.spar	-107.8	2955
208	90.0	fwd	Fwd.spar	98.9	2955
210	0.0	fwd	Fwd.spar	-340.4	2891
211	-45.0	fwd	Fwd.spar	6.1	2891
212	90.0	fwd	Fwd.spar	43.0	2891
213	0.0	fwd	Fwd.spar	-3958.6	3172
214	0.0	fwd	Fwd.spar	-4064.6	2671

Strain prediction from global model at ultimate load of 166,000 lbs.

Strain Gage No	Angle	Surface	Location	Micro Strain	Node Number in FEM Model
215	0.0	fwd	Fwd.spar	-3585.7	2719
216	0.0	fwd	Fwd.spar	-3238.2	2767
217	0.0	fwd	Fwd.spar	-2217.4	2815
218	0.0	fwd	Fwd.spar	-1293.1	2836
301	45.0	fwd	Rear.Spar	66.3	3324
305	45.0	fwd	Rear.Spar	75.5	3307
309	45.0	fwd	Rear.Spar	1023.8	3292
441	0.0	out	RIB.4	267.7	3703
442	45.0	out	RIB.4	-422.5	3703
443	90.0	out	RIB.4	-260.4	3703
449	0.0	out	RIB.4	998.7	3674
451	0.0	out	RIB.5	-185.5	3918
452	45.0	out	RIB.5	532.0	3918
453	90.0	out	RIB.5	292.7	3918
461	0.0	out	Rib.6	133.6	3960
462	-45.0	out	Rib.6	184.2	3960
463	90.0	out	Rib.6	-108.5	3960
469	0.0	out	Rib.6	-549.9	4167
471	0.0	out	Rib.7	-303.4	4348
472	-45.0	out	Rib.7	-149.6	4348
473	90.0	out	Rib.7	211.8	4348
479	0.0	out	Rib.7	-299.5	4250
480	90.0	out	Rib.7	461.0	4334
481	0.0	out	Rib.8	-118.6	4475
482	-45.0	out	Rib.8	-158.8	4475
483	90.0	out	Rib.8	282.8	4475
489	0.0	out	Rib.8	968.9	4507
504	0.0	aft	Ext.Box	178.7	5104
504	0.0	aft	Ext.Box	0.0	5104
505	-45.0	aft	Ext.Box	-2456.7	5104
505	-45.0	aft	Ext.Box	0.0	5104
506	90.0	aft	Ext.Box	-319.2	5104

Table II (Continued)

Strain prediction from global model at ultimate load of 166,000 lbs.

Strain Gage No	Angle	Surface	Location	Micro Strain	Node Number in FEM Model
506	90.0	aft	Ext.Box	0.0	5104
510	0.0	int	Tr.Str.Up	66.3	4865
601	0.0	int	Upr.Skin	-4472.7	387
609	-13.0	int	Upr.Skin	-4525.4	57
141	0.0	ext	Lwr.Skin	3338.4	1452
144	0.0	ext	Lwr.Skin	3288.1	1605
146	0.0	ext	Lwr.Skin	3220.3	1636
148	0.0	ext	Lwr.Skin	3136.2	1674
150	0.0	ext	Lwr.Skin	3038.0	1714
152	0.0	ext	Lwr.Skin	2926.0	1753
154	0.0	ext	Lwr.Skin	2796.6	1800
156	0.0	ext	Lwr.Skin	2623.0	1836

Table III. Srain prediction from global model at 50% of ultimate load (including all gages on external upper skin) .

Strain Gage No	Angle	Surface	Location	Micro Strain	Node Number in FEM Model
2	0.0	ext	Upr.Skin	-1805.0	196
4	0.0	ext	Upr.Skin	-1915.2	194
5	0.0	ext	Upr.Skin	-2428.3	65
6	45.0	ext	Upr.Skin	-827.9	65
7	90.0	ext	Upr.Skin	915.4	65
11	0.0	ext	Upr.Skin	-2430.7	1359
12	0.0	ext	Upr.Skin	-2430.7	1359
15	0.0	ext	Upr.Skin	-2268.3	614
16	0.0	ext	Upr.Skin	-2268.3	614
17	0.0	ext	Upr.Skin	-2239.3	71
18	0.0	ext	Upr.Skin	-2339.6	414
20	0.0	ext	Upr.Skin	-2266.2	437
22	0.0	ext	Upr.Skin	-2105.2	371
25	0.0	ext	Upr.Skin	-2113.0	101
26	0.0	ext	Upr.Skin	-2195.9	403
27	45.0	ext	Upr.Skin	-397.5	403
28	90.0	ext	Upr.Skin	703.7	403
32	0.0	ext	Upr.Skin	-2019.1	401
37	0.0	ext	Upr.Skin	-2299.2	474
39	0.0	ext	Upr.Skin	-2258.8	523
46	0.0	ext	Upr.Skin	-2416.9	885
46	0.0	ext	Upr.Skin	-2416.9	885
48	-13.0	ext	Upr.Skin	-2242.0	47
50	0.0	ext	Upr.Skin	-2342.2	518
51	0.0	ext	Upr.Skin	-2305.2	877
52	45.0	ext	Upr.Skin	-376.4	877
53	90.0	ext	Upr.Skin	738.7	877
58	0.0	ext	Upr.Skin	-1934.7	125

Table III (continued)

Strain prediction from global model at 50% of ultimate load.

Strain Gage No	Angle	Surface	Location	Micro Strain	Node Number in FEM Model
62	0.0	ext	Upr.Skin	-1902.2	872
63	0.0	ext	Upr.Skin	-1984.5	1328
65	0.0	ext	Upr.Skin	-1869.7	864
67	0.0	ext	Upr.Skin	-1518.6	121
69	0.0	int	Int.Coast	596.8	Q3098/99
70	45	int	Int.Coast	430.6	Q3098/99
71	90	int	Int.Coast	-257.5	Q3098/99
72	0.0	ext	Upr.Skin	-1552.5	68
74	-13.0	ext	Upr.Skin	-1402.0	107
75	0.0	ext	Upr.Skin	-2620.2	117
77	-13.0	ext	Upr.Skin	-810.5	221
78	0.0	ext	Upr.Skin	-4011.0	43
79	0.0	ext	Upr.Skin	-3589.1	25
81	0.0	ext	Upr.Skin	-2889.8	62
84	0.0	ext	Upr.Skin	-2308.8	63
92	0.0	ext	Upr.Skin	-2545.0	1234
93	0.0	ext	Upr.Skin	-2751.8	1292
94	0.0	ext	Upr.Skin	-2268.3	614
95	0.0	ext	Upr.Skin	-2268.3	614
96	0.0	ext	Upr.Skin	-2430.7	1359
102	0.0	int	Lwr.Skin	1113.9	1467
123	0.0	int	Lwr.Skin	982.1	2244

Table III (continued)

Strain prediction from global model at 50% of ultimate load.

Strain Gage No	Angle	Surface	Location	Micro Strain	Node Number in FEM Model
125	0.0	int	Lwr.Skin	1238.6	2260
128	0.0	int	Lwr.Skin	1302.9	2276
136	0.0	int	Lwr.Skin	1253.9	1371
140	0.0	int	Lwr.Skin	1554.2	1452
144	0.0	ext	Lwr.Skin	1586.5	1605
201	-45.0	aft	Fwd.spar	-117.9	3007
205	-45.0	aft	Fwd.spar	-63.4	2955
209	-45.0	aft	Fwd.spar	2891.0	302
303	45.0	aft	Rear.Spar	21.2	3324
304	90.0	aft	Rear.Spar	176.3	3324
306	0.0	aft	Rear.Spar	-398.8	3307
307	45.0	aft	Rear.Spar	60.0	3307
308	90.0	aft	Rear.Spar	170.3	3307
310	0.0	aft	Rear.Spar	-94.9	3292
311	45.0	aft	Rear.Spar	518.7	3292
312	90.0	aft	Rear.Spar	-198.3	3292
444	45.0	inb	RIB.4	-189.3	3703
445	90.0	inb	RIB.4	15.0	3651
448	0.0	inb	RIB.4	492.7	3674
454	45.0	inb	RIB.5	289.8	3918
455	90.0	inb	RIB.5	43.6	3823
464	-45.0	inb	Rib.6	111.4	3960
465	90.0	inb	Rib.6	57.2	3961
468	0.0	inb	Rib.6	-174.2	4167
474	-45.0	inb	Rib.7	-39.2	4348
475	90.0	inb	Rib.7	65.9	4173
478	0.0	inb	Rib.7	-101.9	4250
484	-45.0	inb	Rib.8	-105.1	4475
485	90.0	inb	Rib.8	61.7	4382
488	0.0	inb	Rib.8	328.2	4507
501	0.0	fwd	Ext.Box	79.5	5104

Table III (continued)

Strain prediction from global model at 50% of ultimate load.

Strain Gage No	Angle	Surface	Location	Micro Strain	Node Number in FEM Model
502	-45.0	fwd	Ext.Box	-1240.2	5104
503	90.0	fwd	Ext.Box	-157.4	5104
507	0.0	Int	Ext.Box	161.6	Q4160
511	0.0	ext	Tr.Str.Up	27.0	4852
513	0.0	ext	Tr.Str.Up	23.2	4865
602	0.0	ext	Upr.Skin	-2317.1	387
604	0.0	ext	Upr.Skin	-2322.1	421
606	0.0	ext	Upr.Skin	-2191.3	453
610	-13.0	ext	Upr.Skin	-810.5	221
611	0.0	ext	Upr.Skin	-1995.0	49
612	0.0	ext	Upr.Skin	-4073.9	39
613	0.0	ext	Upr.Skin	-1626.0	120
614	0.0	ext	Upr.Skin	-1795.9	69
615	0.0	ext	Upr.Skin	-2237.3	444
616	0.0	ext	Upr.Skin	-2221.1	449
617	0.0	ext	Upr.Skin	-2416.8	885

Table IV. Strain prediction from global model at 50% of ultimate load (including all gages on internal upper skin).

Strain Gage No	Angle	Surface	Location	Micro Strain	Node Number in FEM Model
1	0.0	int	Upr.Skin	-2001.4	196
3	0.0	int	Upr.Skin	-2206.4	194
9	0.0	int	Upr.Skin	-2358.6	1359
10	0.0	int	Upr.Skin	-2358.6	1359
13	0.0	int	Upr.Skin	-2172.0	614
14	0.0	int	Upr.Skin	-2172.0	614
30	90.0	int	Upr.Skin	-2119.2	399
31	0.0	int	Upr.Skin	-2014.1	401
33	0.0	int	Upr.Skin	137.0	4336
34	45.0	int	Upr.Skin	154.1	4336
35	90.0	int	Upr.Skin	259.7	4336
36	0.0	int	Upr.Skin	-2134.3	474
38	0.0	int	Upr.Skin	-2185.8	523
40	0.0	int	Upr.Skin	245.7	4388
41	45.0	int	Upr.Skin	109.7	4388
42	90.0	int	Upr.Skin	298.1	4388
43	0.0	int	Upr.Skin	-2535.9	885
44	0.0	int	Upr.Skin	-2535.9	885
47	-103.0	int	Upr.Skin	890.6	493
64	0.0	int	Upr.Skin	-1761.1	1328
68	0.0	int	Upr.Skin	-1613.7	121
80	0.0	int	Upr.Skin	-2970.6	25
87	0.0	int	Upr.Skin	-2547.4	1292
91	0.0	int	Upr.Skin	-2570.4	1234
101	0.0	ext	Lwr.Skin	1291.5	1496
103	0.0	ext	Lwr.Skin	1402.1	1550
104	45.0	ext	Lwr.Skin	247.8	1550

Table IV (continued)

Strain prediction from global model at 50% of ultimate load.

Strain Gage No	Angle	Surface	Location	Micro Strain	Node Number in FEM Model
105	90.0	ext	Lwr.Skin	-540.1	1550
107	0.0	ext	Lwr.Skin	1330.0	1667
109	0.0	ext	Lwr.Skin	1670.2	1558
111	0.0	ext	Lwr.Skin	1450.6	1574
112	45.0	ext	Lwr.Skin	490.9	1574
113	90.0	ext	Lwr.Skin	-522.7	1574
115	0.0	ext	Lwr.Skin	1486.0	1446
116	0.0	ext	Lwr.Skin	1278.0	1691
118	0.0	ext	Lwr.Skin	1157.6	1784
119	45.0	ext	Lwr.Skin	290.1	1784
120	90.0	ext	Lwr.Skin	-361.1	1784
122	13.0	ext	Lwr.Skin	312.2	1385
124	13.0	ext	Lwr.Skin	694.3	1374
126	0.0	ext	Lwr.Skin	1181.3	2273
129	0.0	ext	Lwr.Skin	1315.3	2287
131	0.0	ext	Lwr.Skin	1323.5	1808
132	45.0	ext	Lwr.Skin	217.2	1808
133	90.0	ext	Lwr.Skin	-416.9	1808
137	13.0	ext	Lwr.Skin	1057.0	1371
138	0.0	ext	Lwr.Skin	1469.8	2276
139	0.0	ext	Lwr.Skin	1533.8	2291
202	0.0	fwd	Fwd.spar	-333.0	3007
203	-45.0	fwd	Fwd.spar	-165.7	3007
204	90.0	fwd	Fwd.spar	-290.8	2007
206	0.0	fwd	Fwd.spar	-253.6	2955
207	-45.0	fwd	Fwd.spar	-66.6	2955
208	90.0	fwd	Fwd.spar	44.5	2955
210	0.0	fwd	Fwd.spar	-158.0	2891

Table IV (continued)

Strain prediction from global model at 50% of ultimate load.

Strain Gage No	Angle	Surface	Location	Micro Strain	Node Number in FEM Model
211	-45.0	fwd	Fwd.spar	17.9	2891
212	90.0	fwd	Fwd.spar	15.4	2891
213	0.0	fwd	Fwd.spar	-2038.8	3172
214	0.0	fwd	Fwd.spar	-2017.9	2671
215	0.0	fwd	Fwd.spar	-1712.9	2719
216	0.0	fwd	Fwd.spar	-1526.5	2767
217	0.0	fwd	Fwd.spar	-1087.3	2815
218	0.0	fwd	Fwd.spar	-618.9	2836
301	45.0	fwd	Rear.Spar	34.1	3324
305	45.0	fwd	Rear.Spar	54.8	3307
309	45.0	fwd	Rear.Spar	521.4	3292
441	0.0	out	RIB.4	125.3	3703
442	45.0	out	RIB.4	-196.2	3703
443	90.0	out	RIB.4	-32.2	3703
449	0.0	out	RIB.4	515.8	3674
451	0.0	out	RIB.5	-89.3	3918
452	45.0	out	RIB.5	294.0	3918
453	90.0	out	RIB.5	170.6	3918
461	0.0	out	Rib.6	84.5	3960
462	-45.0	out	Rib.6	111.4	3960
463	90.0	out	Rib.6	-39.4	3960
469	0.0	out	Rib.6	-300.4	4167
471	0.0	out	Rib.7	-77.0	4348
472	-45.0	out	Rib.7	-34.7	4348
473	90.0	out	Rib.7	106.8	4348
479	0.0	out	Rib.7	-161.3	4250
480	90.0	out	Rib.7	206.8	4334
481	0.0	out	Rib.8	-57.2	4475

Table IV (continued)

Strain prediction from global model at 50% of ultimate load.

Strain Gage No	Angle	Surface	Location	Micro Strain	Node Number in FEM Model
482	-45.0	out	Rib.8	-95.9	4475
483	90.0	out	Rib.8	154.2	4475
489	0.0	out	Rib.8	569.8	4507
504	0.0	aft	Ext.Box	86.1	5104
504	0.0	aft	Ext.Box	0.0	5104
505	-45.0	aft	Ext.Box	-1233.4	5104
505	-45.0	aft	Ext.Box	0.0	5104
506	90.0	aft	Ext.Box	-158.9	5104
506	90.0	aft	Ext.Box	0.0	5104
510	0.0	int	Tr.Str.Up	32.6	4865
601	0.0	int	Upr.Skin	-2222.2	387
609	-13.0	int	Upr.Skin	-2495.9	57
141	0.0	ext	Lwr.Skin	1654.5	1452
144	0.0	ext	Lwr.Skin	1648.8	1605
146	0.0	ext	Lwr.Skin	1615.9	1636
148	0.0	ext	Lwr.Skin	1573.7	1674
150	0.0	ext	Lwr.Skin	1524.6	1714
152	0.0	ext	Lwr.Skin	1469.5	1753
154	0.0	ext	Lwr.Skin	1405.9	1800
156	0.0	ext	Lwr.Skin	1315.9	1836

Table V Strain estimation from local model at ultimate load of 166,000 lbs.

Strain Gage No	Angle	Surface	Micro Strain	Node
22	0	Ext	-4876.50	18
23	0	IntINB	-147.00	E2000
24	0	IntOUT	77.50	E2000
33	0	Int	977.50	E2415
34	0	Int	-889.50	E2415
35	0	Int	-983.00	E2415
43	0	Int	-4366.50	1184
44	0	Int	-5001.50	1203
45	0	Int	-4743.25	1214
46	0	Ext	-6061.00	1212
48	-13	Ext	-5105.34	239
49	0	INT	-2271.07	506
50	0	Ext	-4257.25	504
51	0	Ext	-4248.00	402
52	45	Ext	-2437.13	402
53	90	Ext	1269.75	402
54	0	INT	-2027.92	506
55	0	Int	-5002.50	2643
56	0	Int	-6058.50	2613
57	0	Int	-5410.00	751
58	0	Ext	-3949.00	498
59	0	Int	-3914.75	1886
60	0	Int	-4370.50	676
61	0	Int	-4668.25	1891
62	0	Ext	-3997.00	679
63	0	Ext	-4312.00	1512
64	0	Int	-3233.25	1512
65	0	Ext	-4410.50	1296
66	0	IntINB	-930.00	E2130
607	0	IntINB	1699.00	E2070
608	0	Ext	-4680.00	468
609	-13	Int	-3072.17	242
617	0	Ext	-5320.50	2148

Table VI Strain estimation from local model at 83,000 lbs (50% Loading)

Strain Gage No	Angle	Surface	Micro Strain	Node
22	0	Ext	-2533.00	18
23	0	IntINB	-22.50	E2000
24	0	IntOUT	-62.50	E2000
33	0	Int	457.00	E2415
34	0	Int	-442.50	E2415
35	0	Int	-480.00	E2415
43	0	Int	-2454.75	1184
44	0	Int	-2784.50	1203
45	0	Int	-2585.00	1214
46	0	Ext	-3292.00	1212
48	-13	Ext	-2807.77	239
49	0	INT	-1231.50	506
50	0	Ext	-2275.25	504
51	0	Ext	-2277.25	402
52	45	Ext	-1212.63	402
53	90	Ext	694.25	402
54	0	INT	-1436.50	506
55	0	Int	-2670.00	2643
56	0	Int	-3227.00	2613
57	0	Int	-2928.00	751
58	0	Ext	-2248.50	498
59	0	Int	-2150.25	1886
60	0	Int	-2553.50	676
61	0	Int	-2434.25	1891
62	0	Ext	-2276.00	679
63	0	Ext	-2271.25	1512
64	0	Int	-1999.50	1512
65	0	Ext	-2148.50	1296
66	0	IntINB	-867.50	E2130
607	0	IntINB	-332.00	E2070
608	0	Ext	-2246.25	468
609	-13	Int	-1665.24	242
617	0	Ext	-2867.50	2148

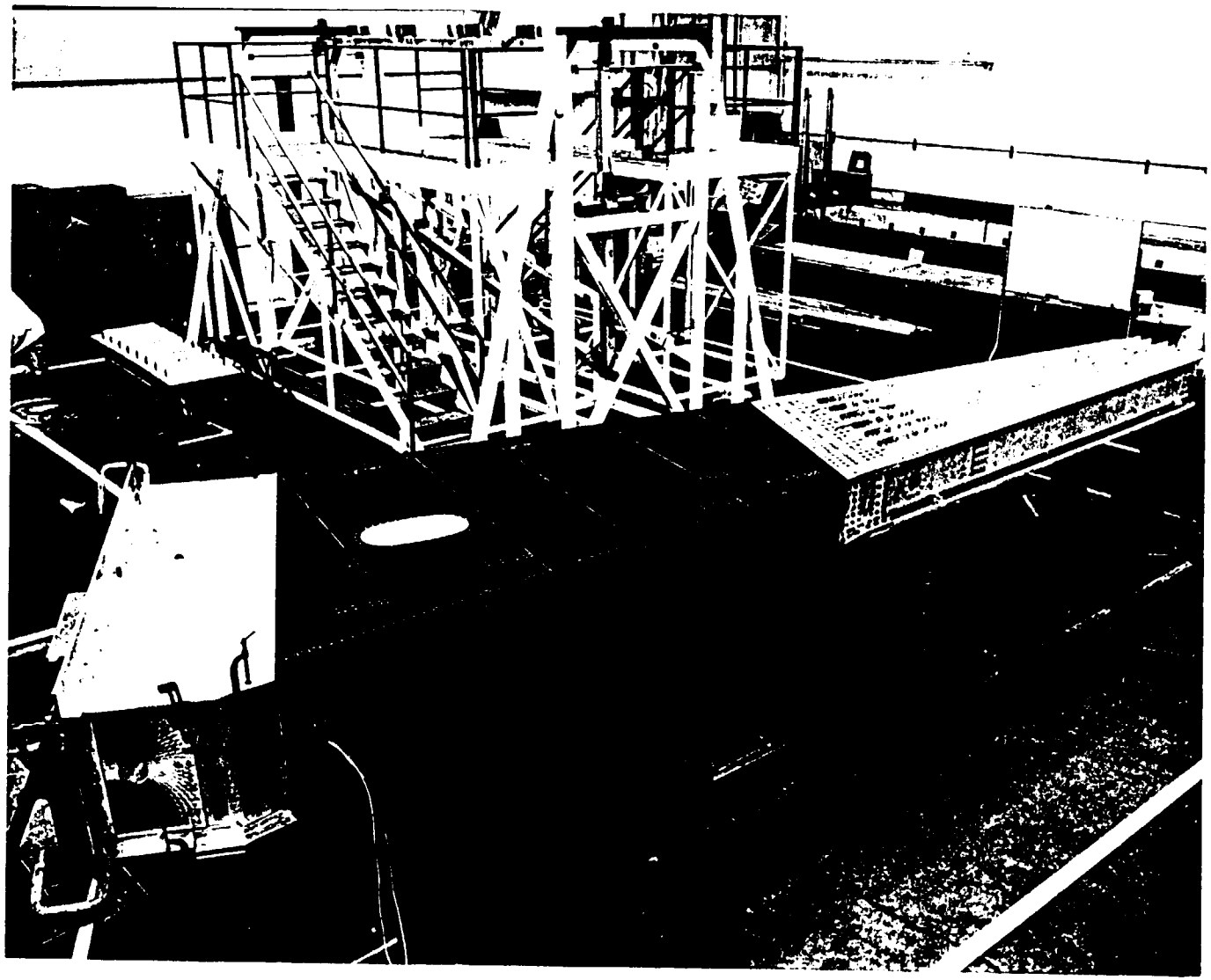

Figure 1. Photograph of McDonnell Douglas wing box test article.

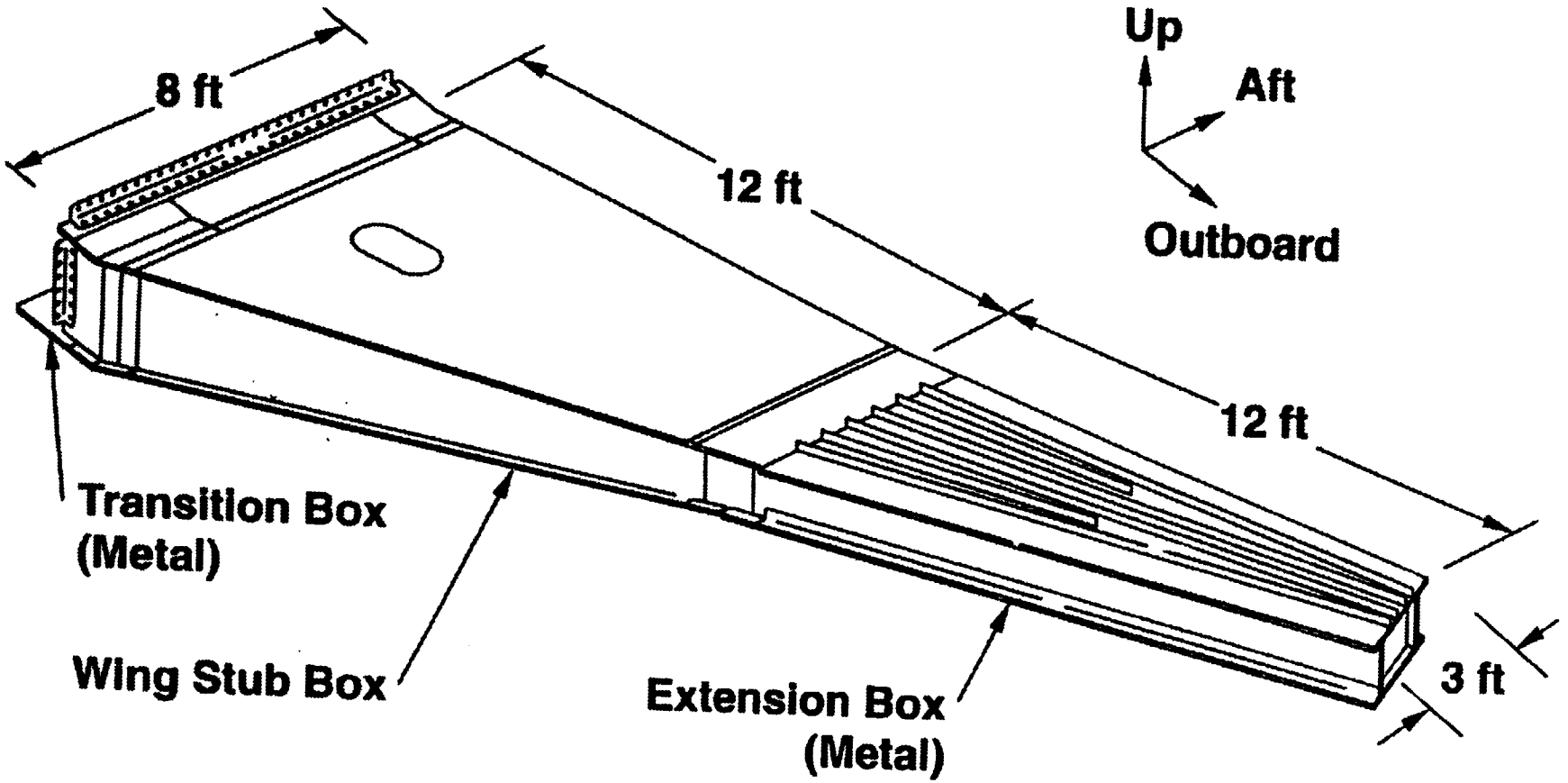

Figure 2. Dimensions of McDonnell Douglas wing box test article.

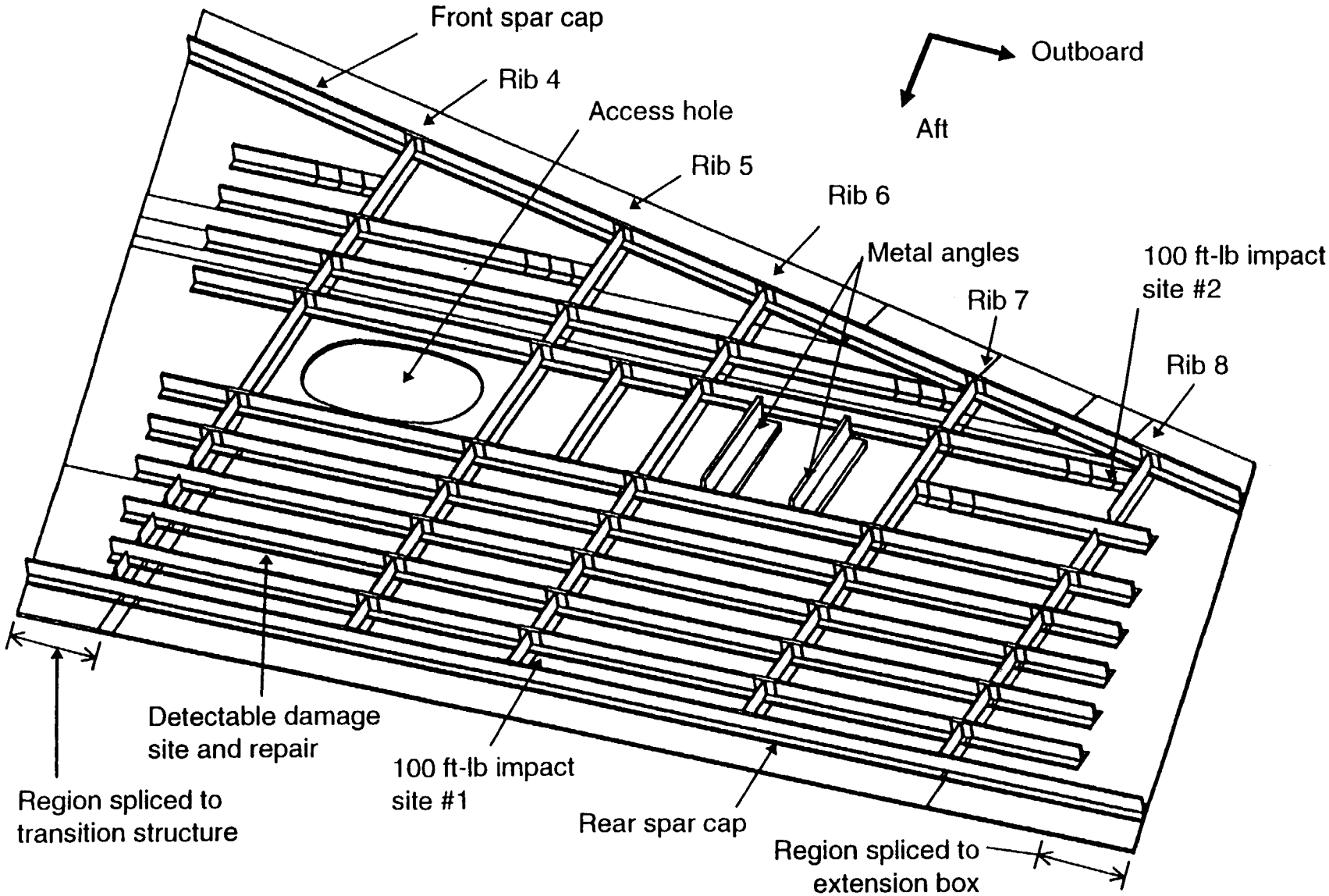

Figure 3. Upper skin panel construction.

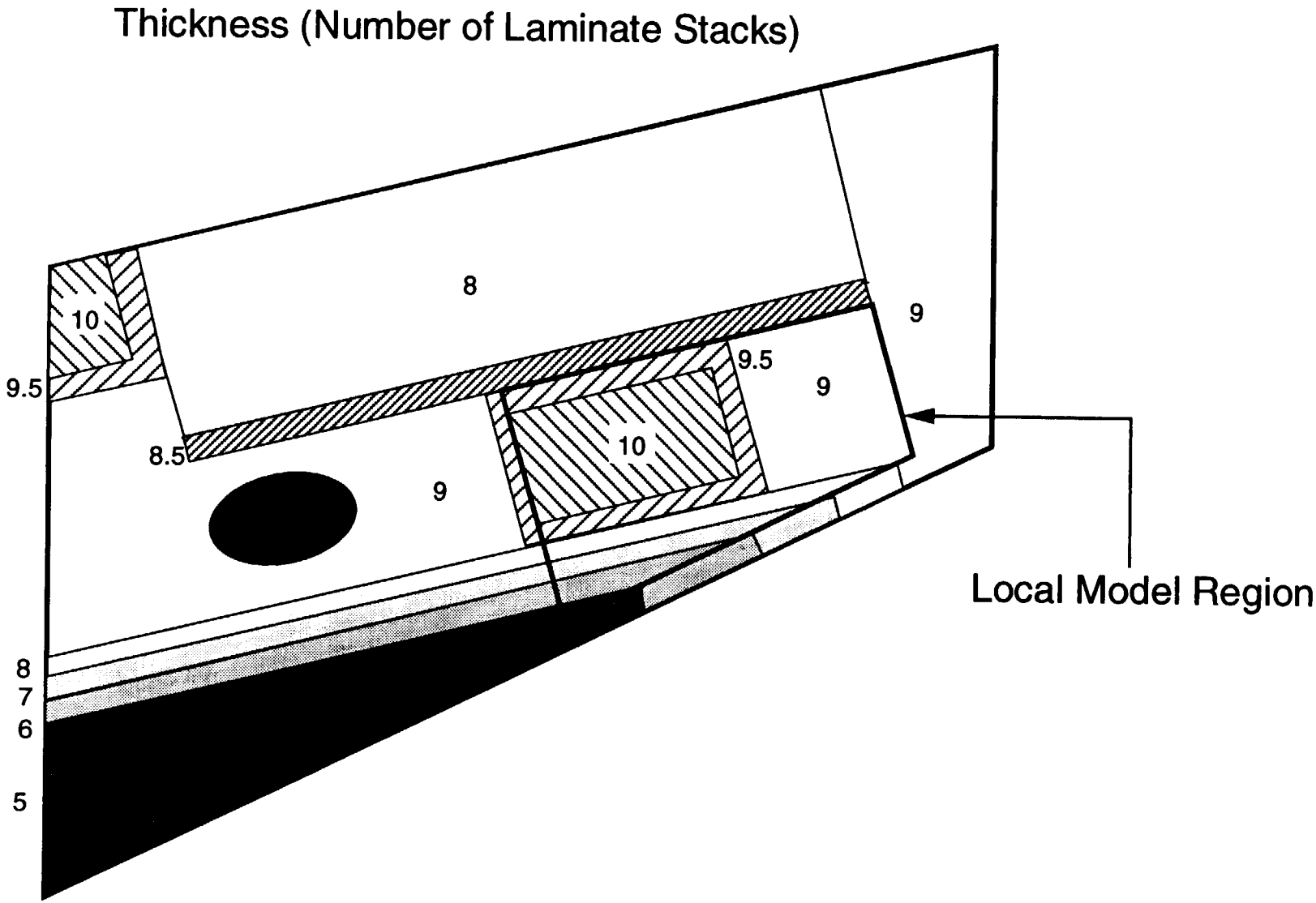

Figure 4. Stub box upper cover thickness distribution.

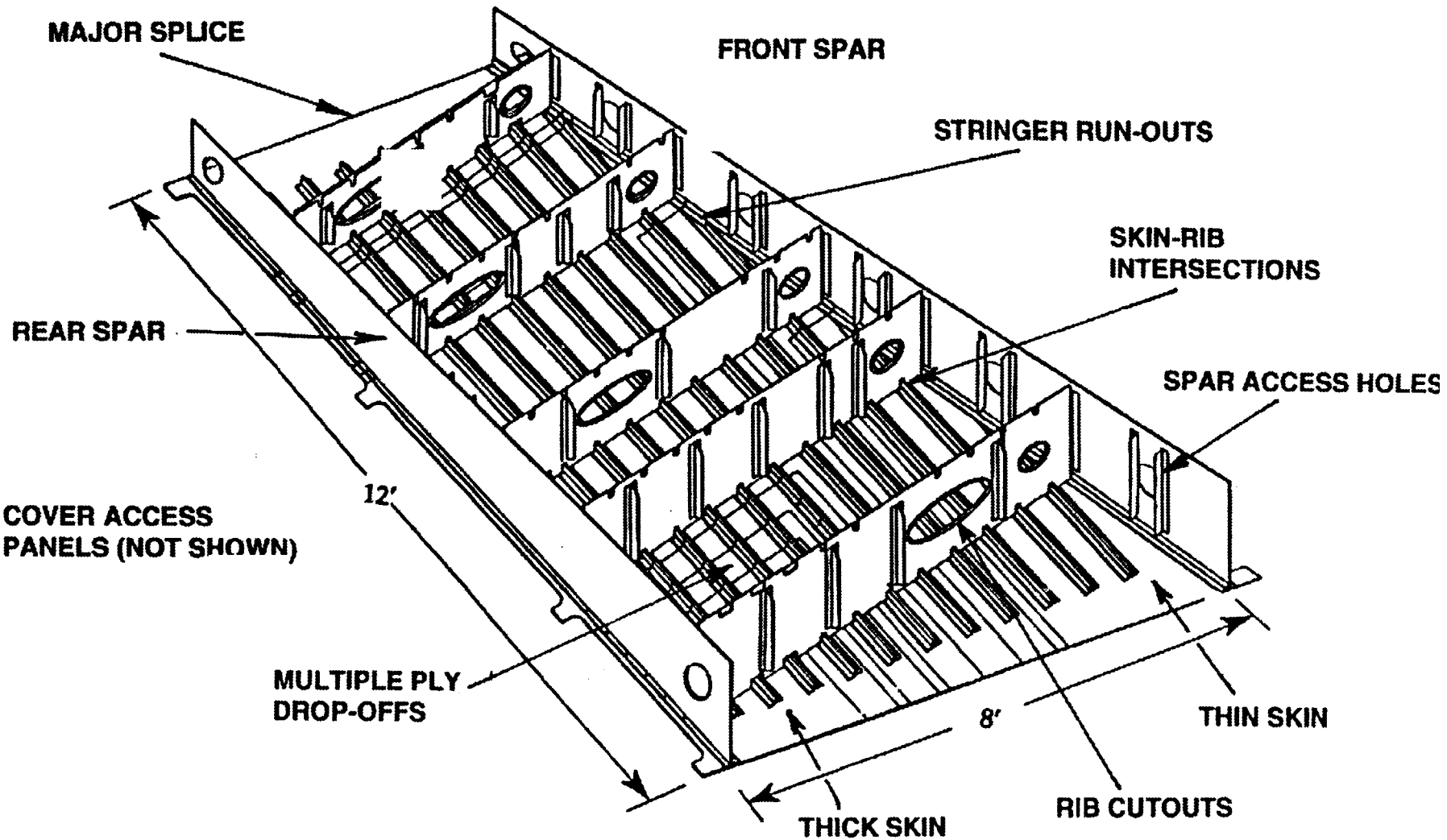

Figure 5. Interior of the composite stub box.

Element Type	No.
CQUAD	4408
CTRIA	99
CBEAM	1308
CONROD	798
RBAR	742
Total No. of Nodes : 5266	

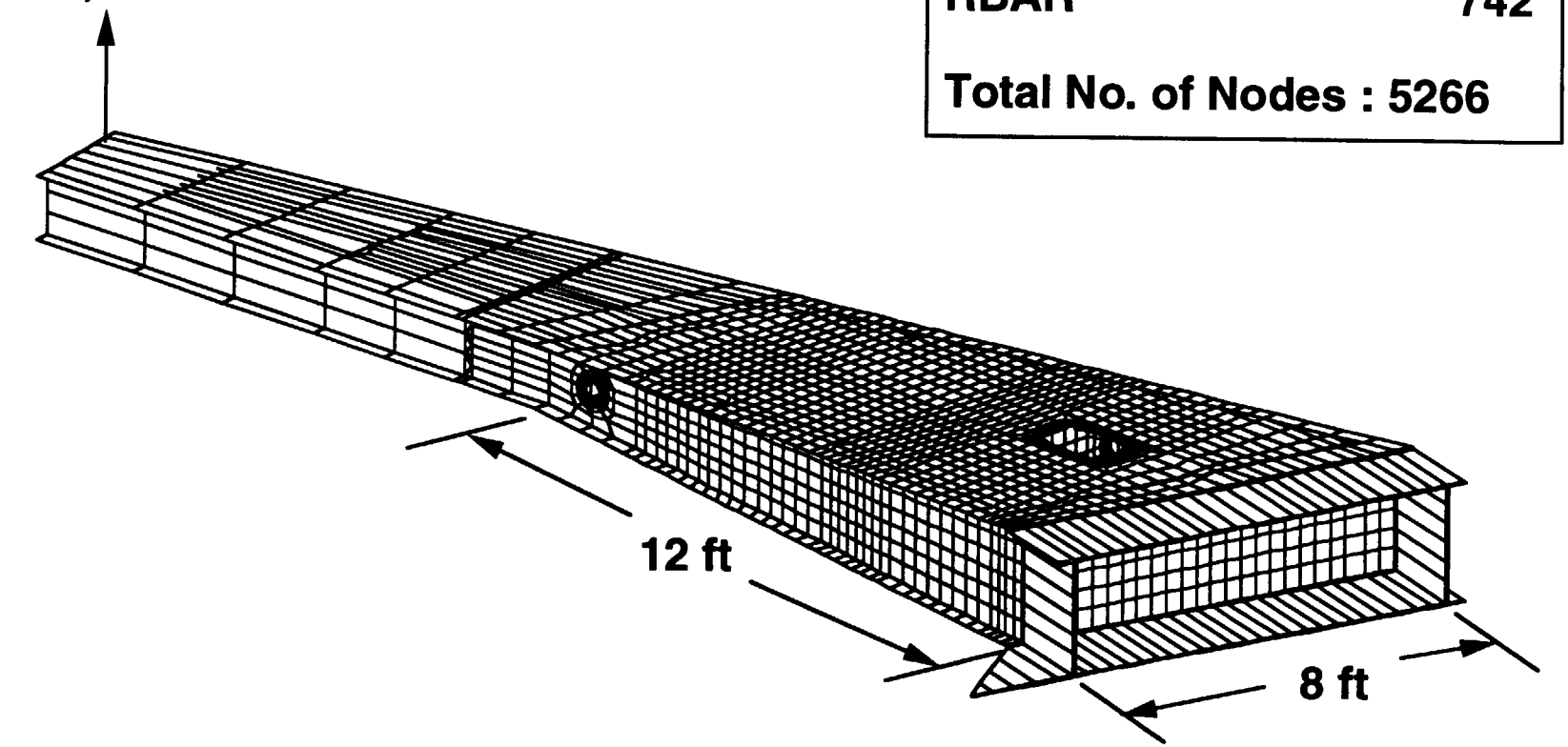

Figure 6. Finite element model of McDonnell Douglas composite wing stub box.

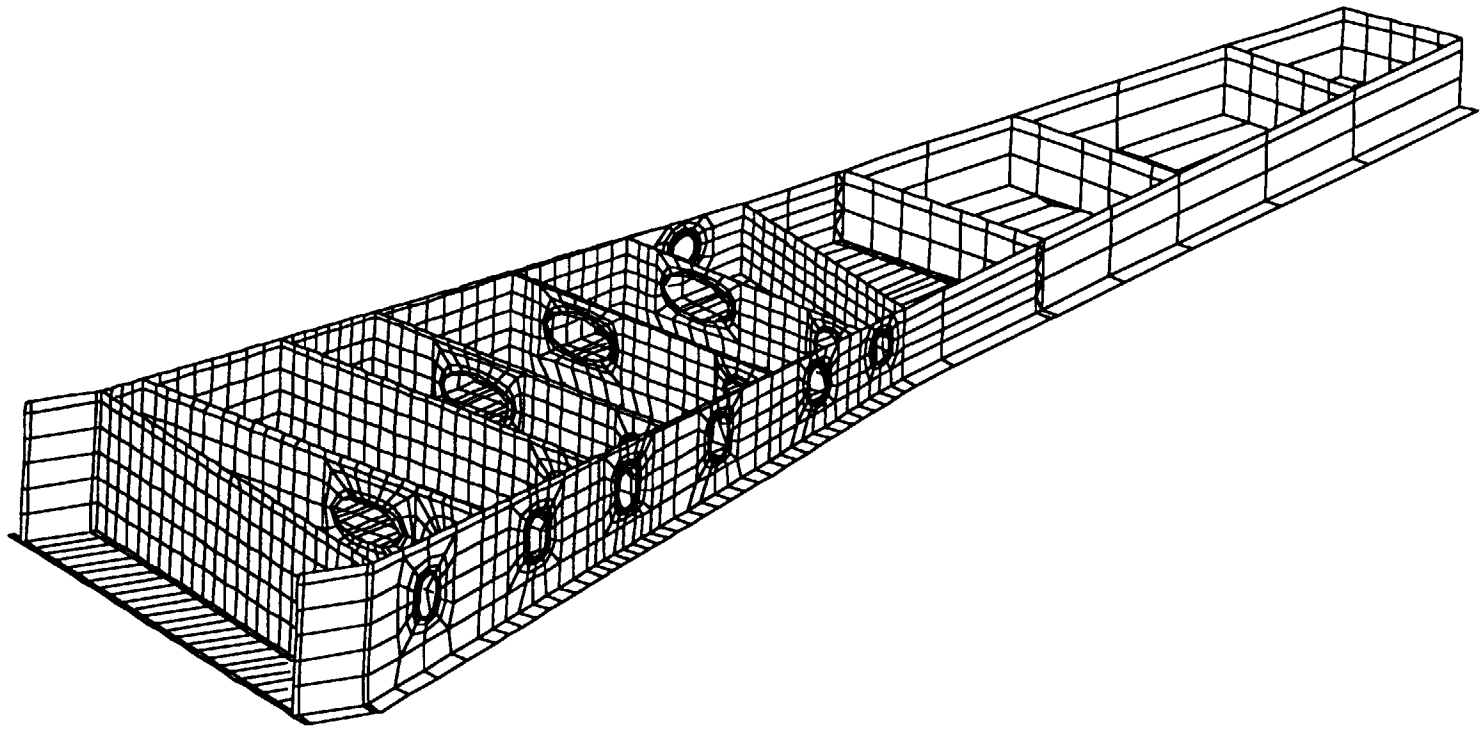

Figure 7. Interior of the stub box finite element model.

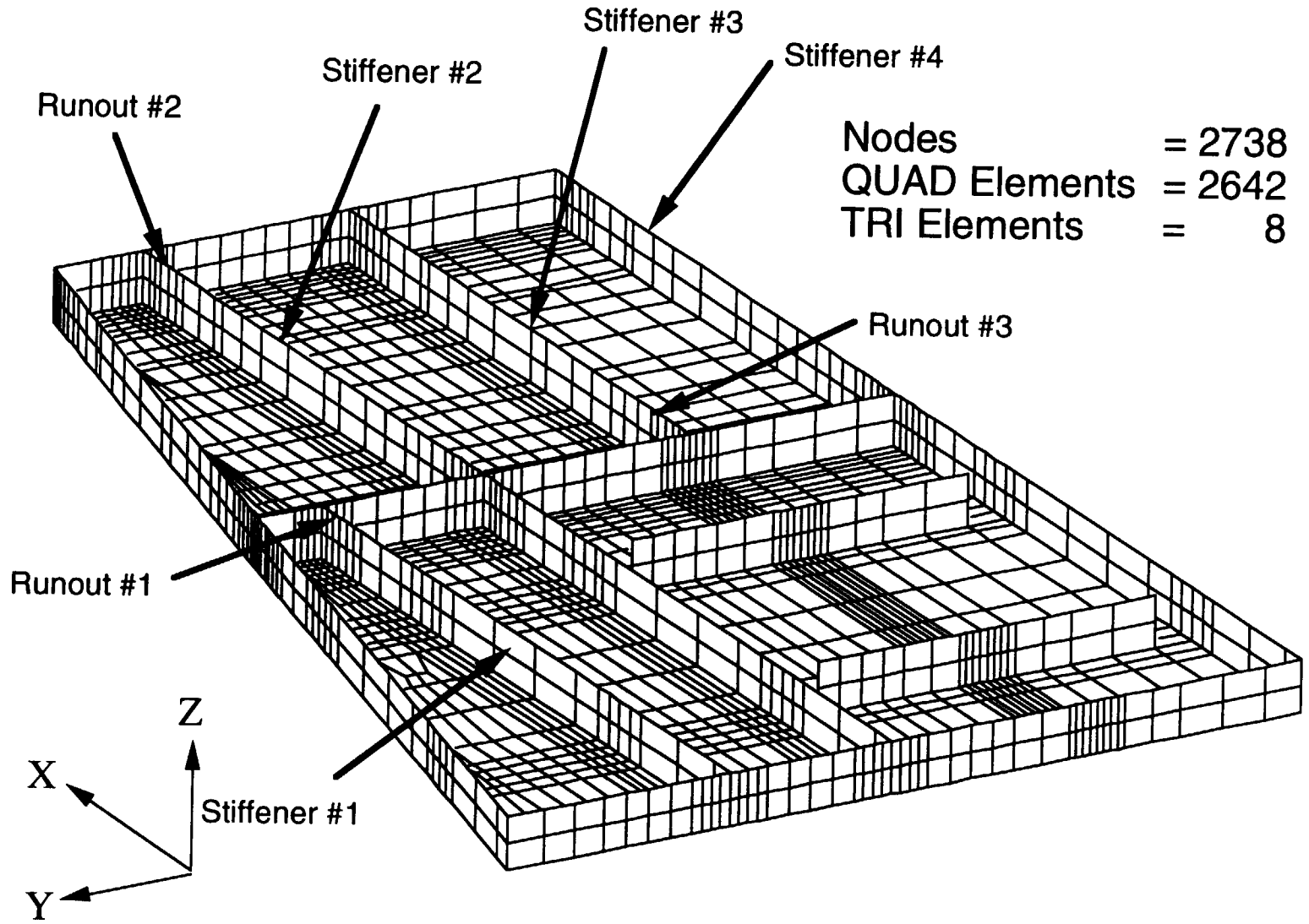

Figure 8. Local finite element model of wing stub box.

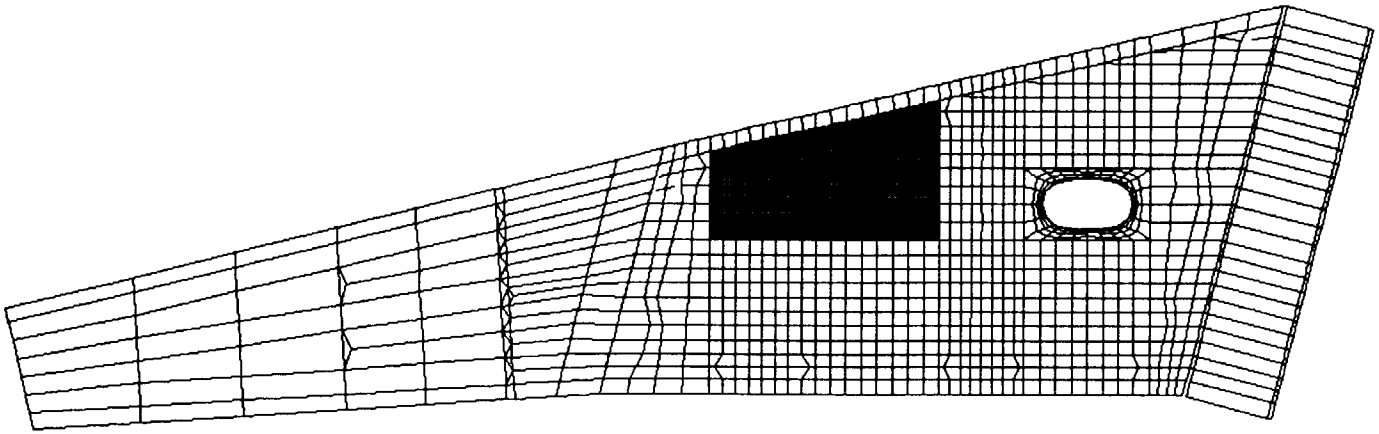

Top View - Local Model Superimposed on Global Model

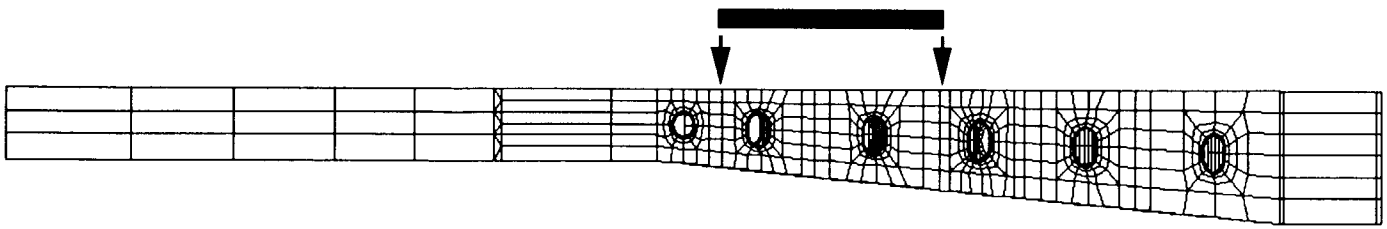

Side View - Local Model Removed from Global Model

Figure 9. Position of local model in the global wing stub box model.

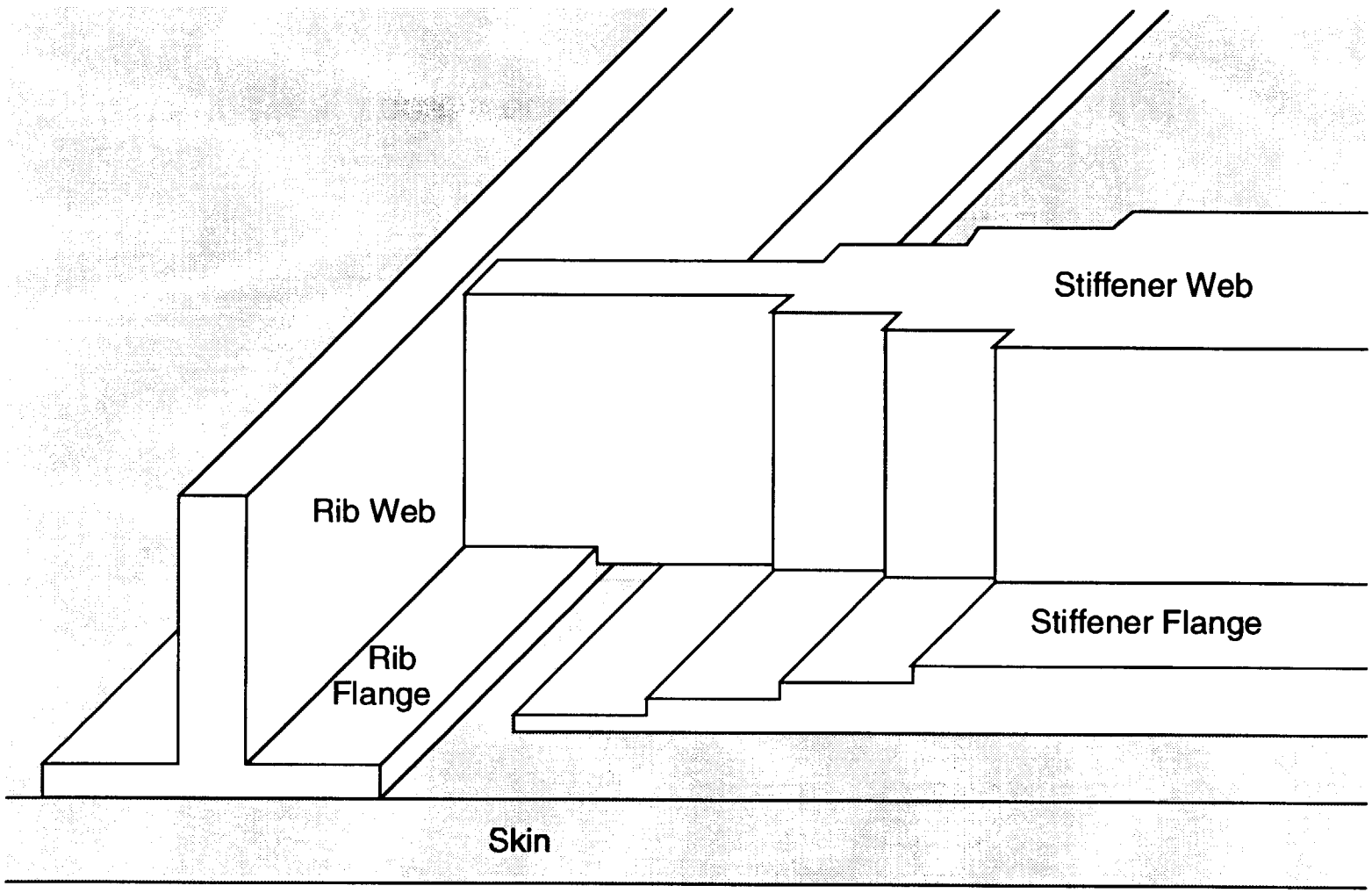

Figure 10. Details of stiffener runout region.

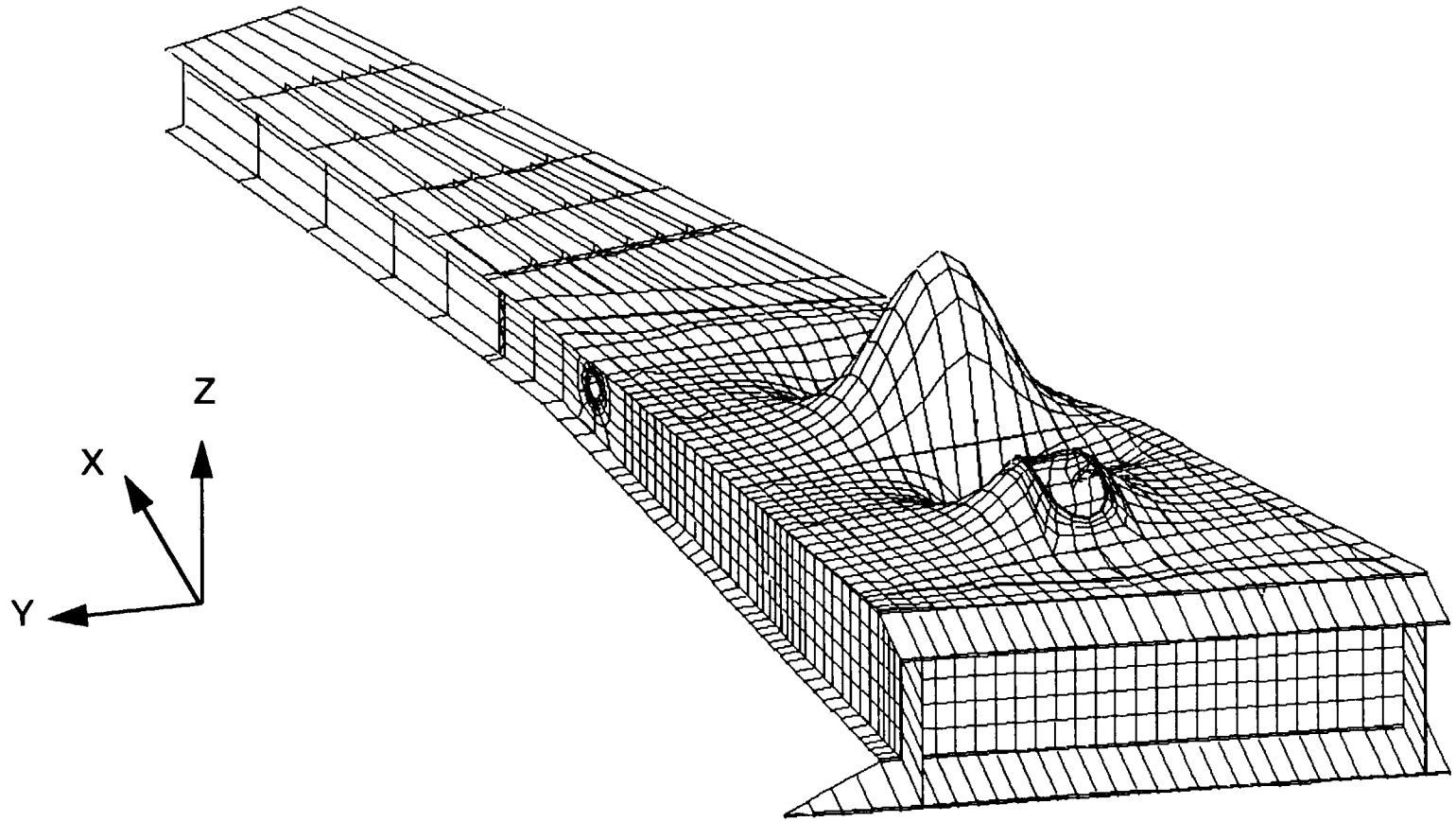

Figure 11. Buckling mode of composite wing box.

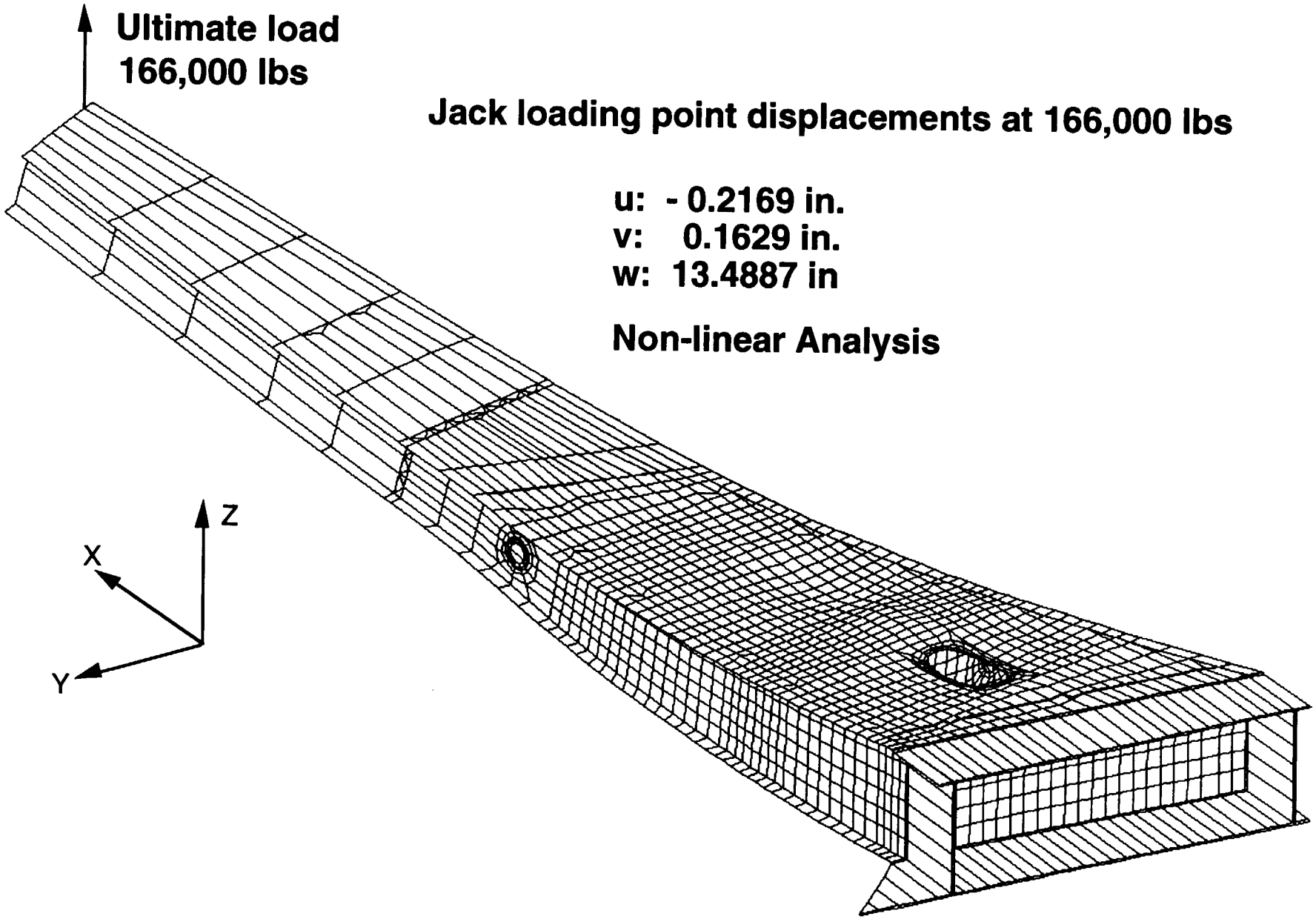

Figure 12. Deformed shape of the global model.

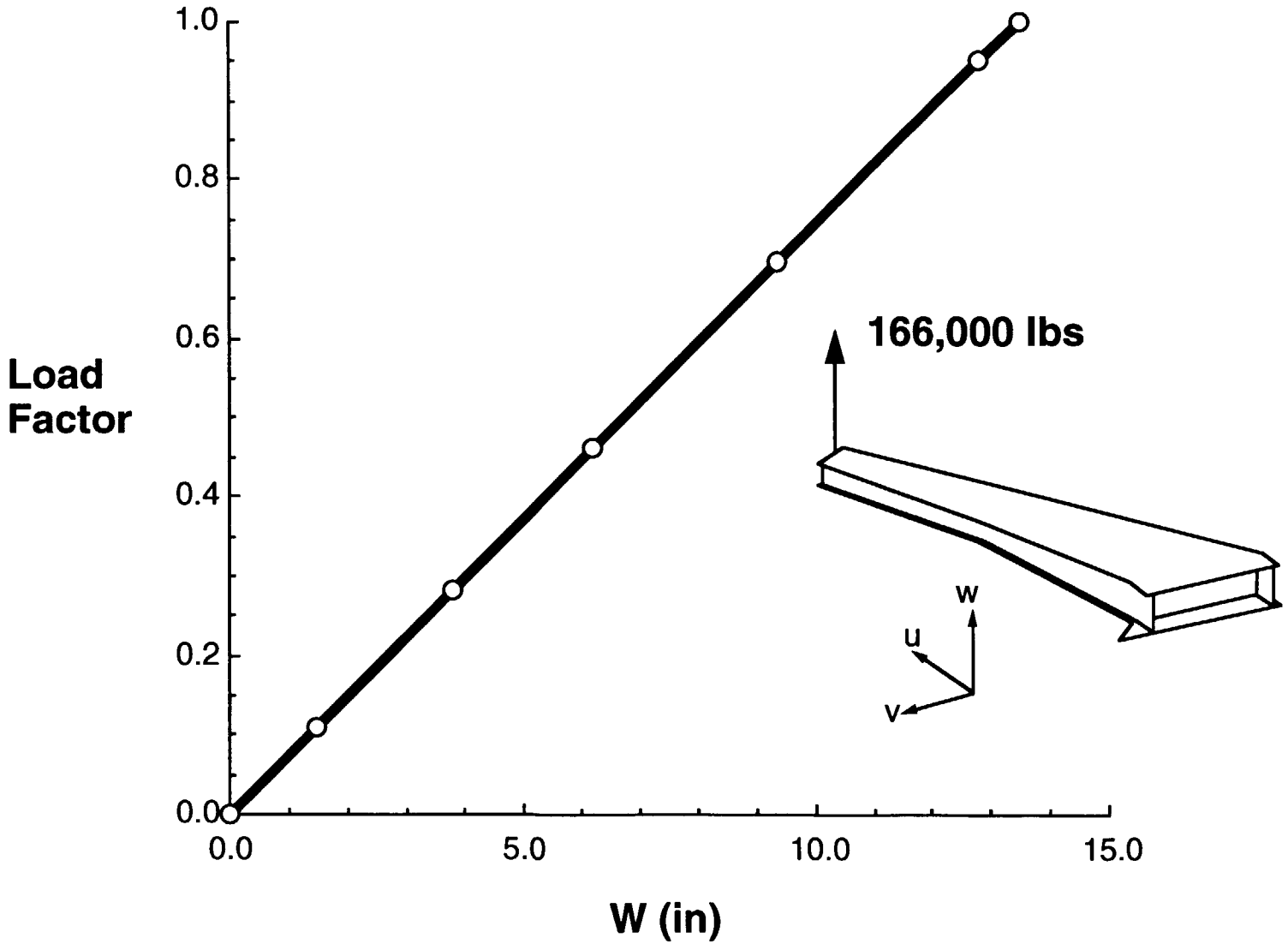

Figure 13. Vertical deflection at load application point.

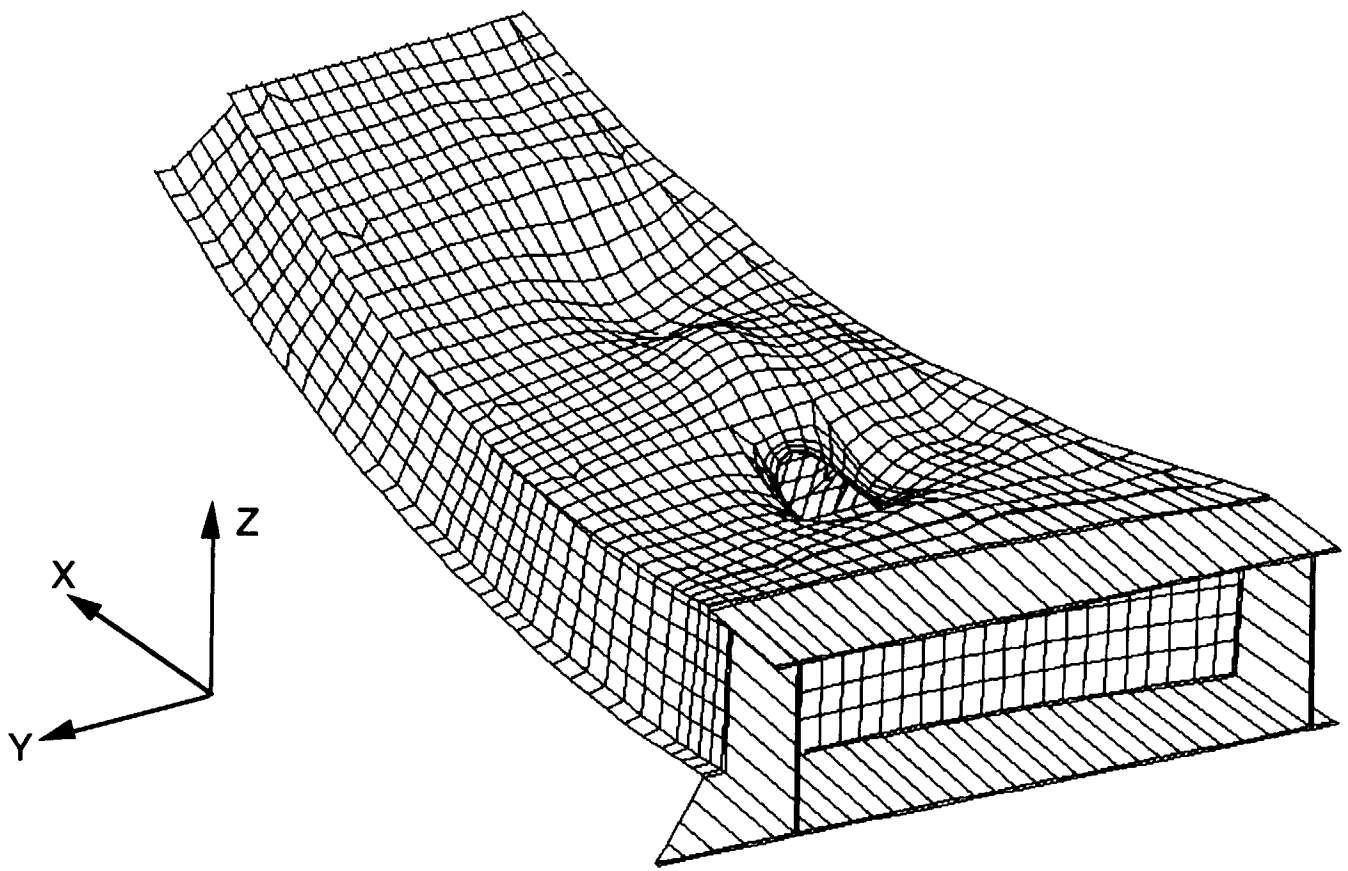

Figure 14. Deformed composite box model due to 166,000 lb. tip load.

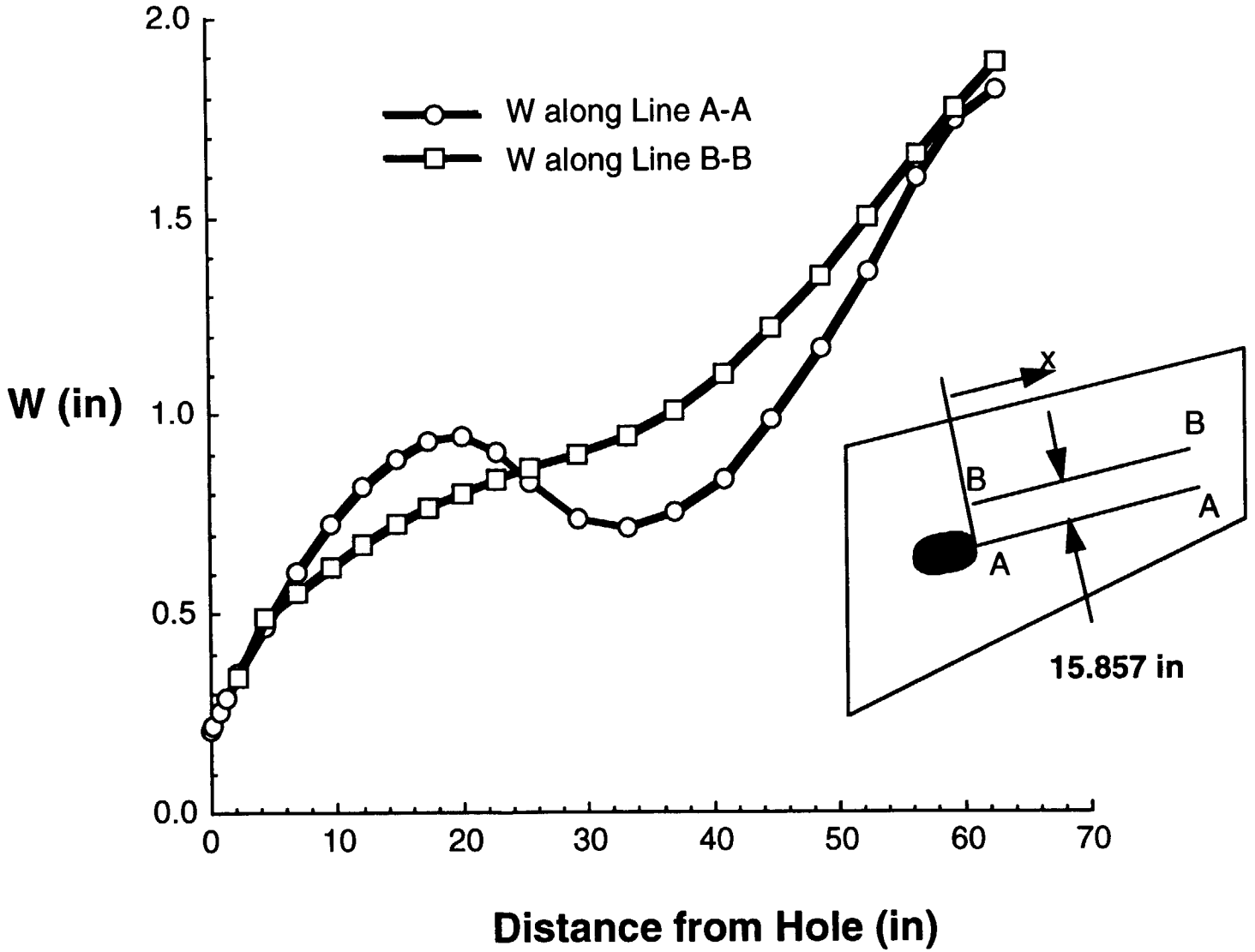

Figure 15. Top cover out-of-plane displacements due to 166,000 lb. tip load.

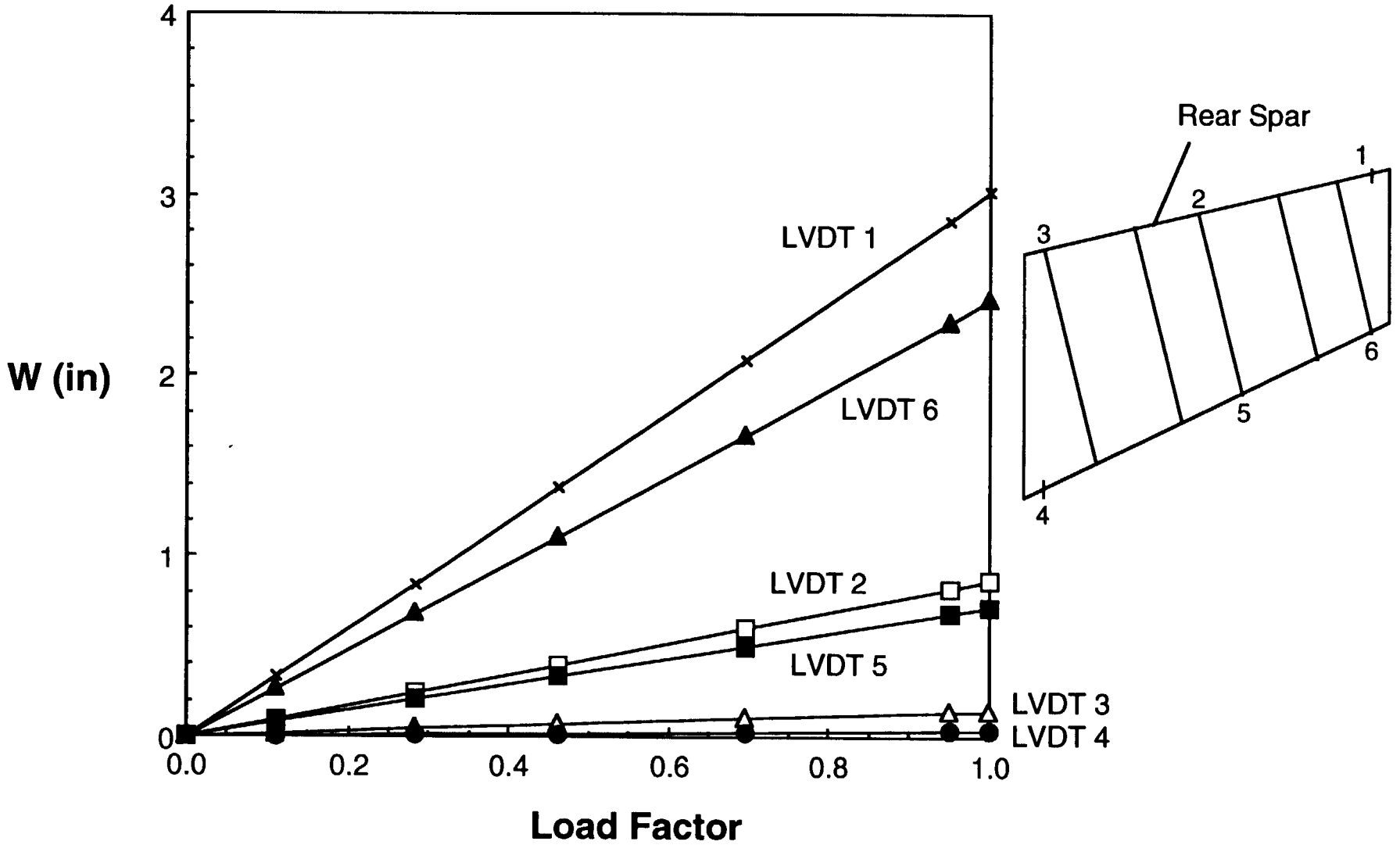

Figure 16. Lower skin out-of-plane displacements at instrumented locations due to 166,000 lb. tip load.

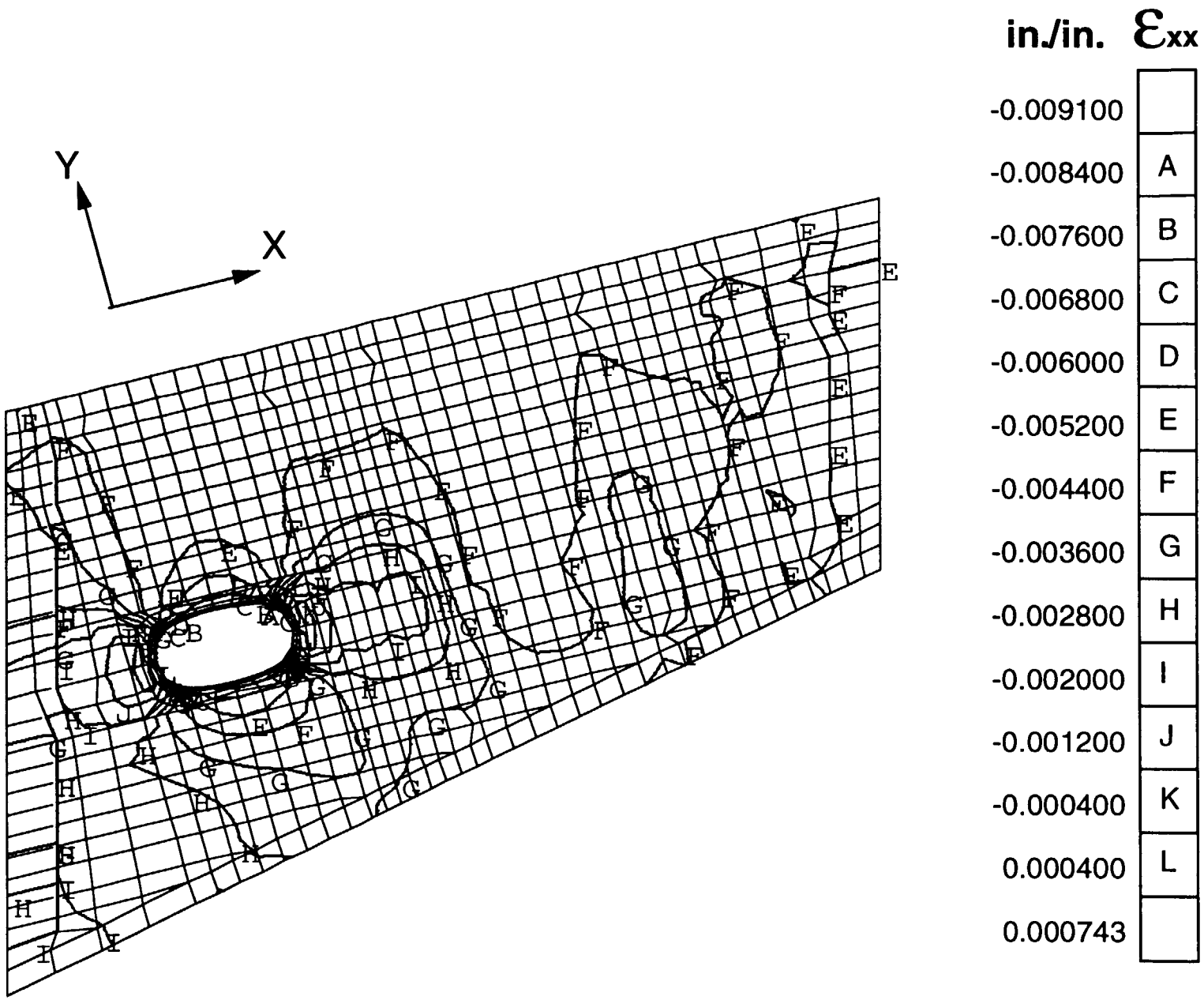

Figure 17. Predicted longitudinal strain contours at skin-side surface of upper cover due to 166,000 lb. tip load.

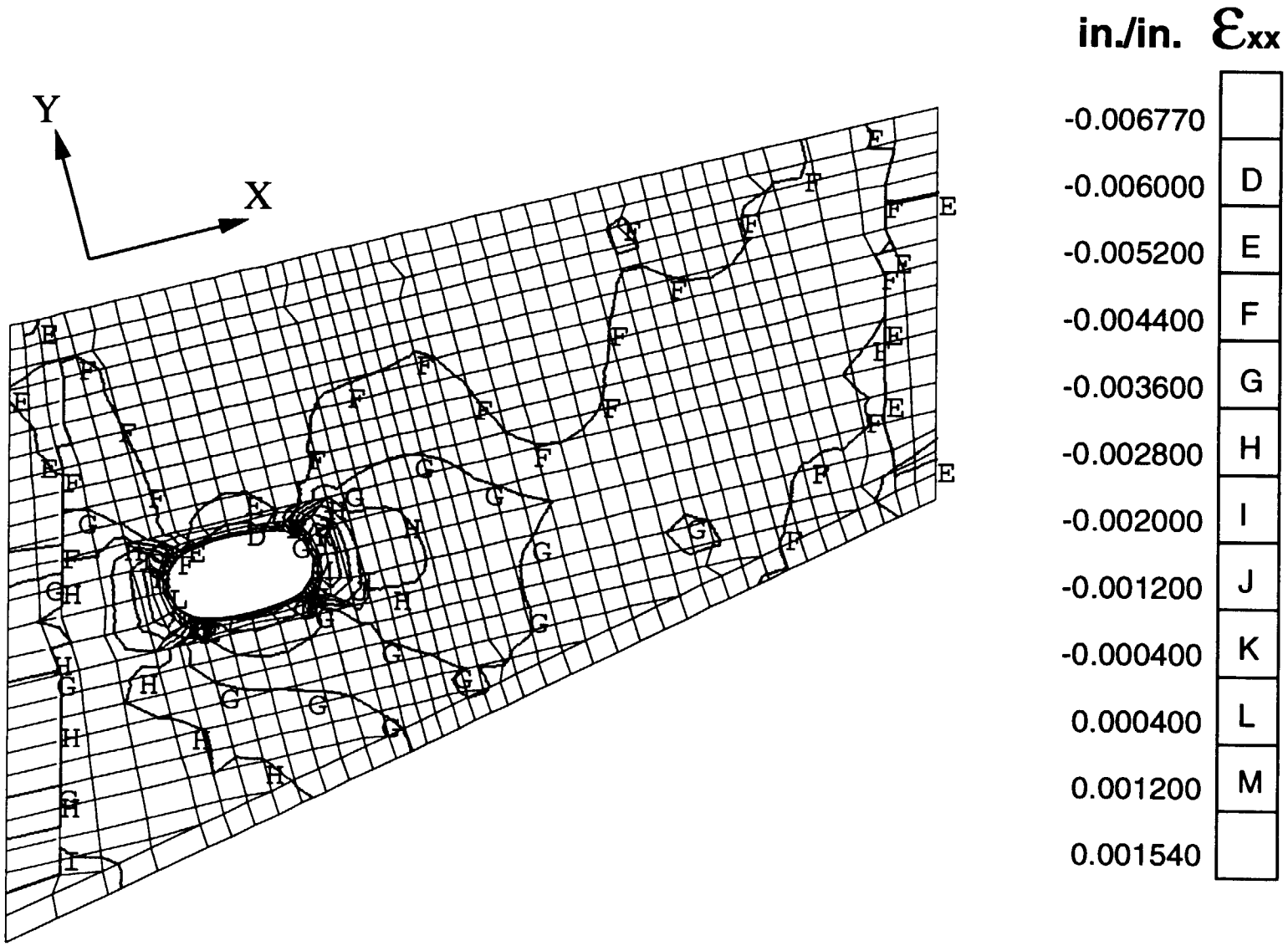

Figure 18. Predicted longitudinal strain contours at middle surface of upper cover due to 166,000 lb. tip load.

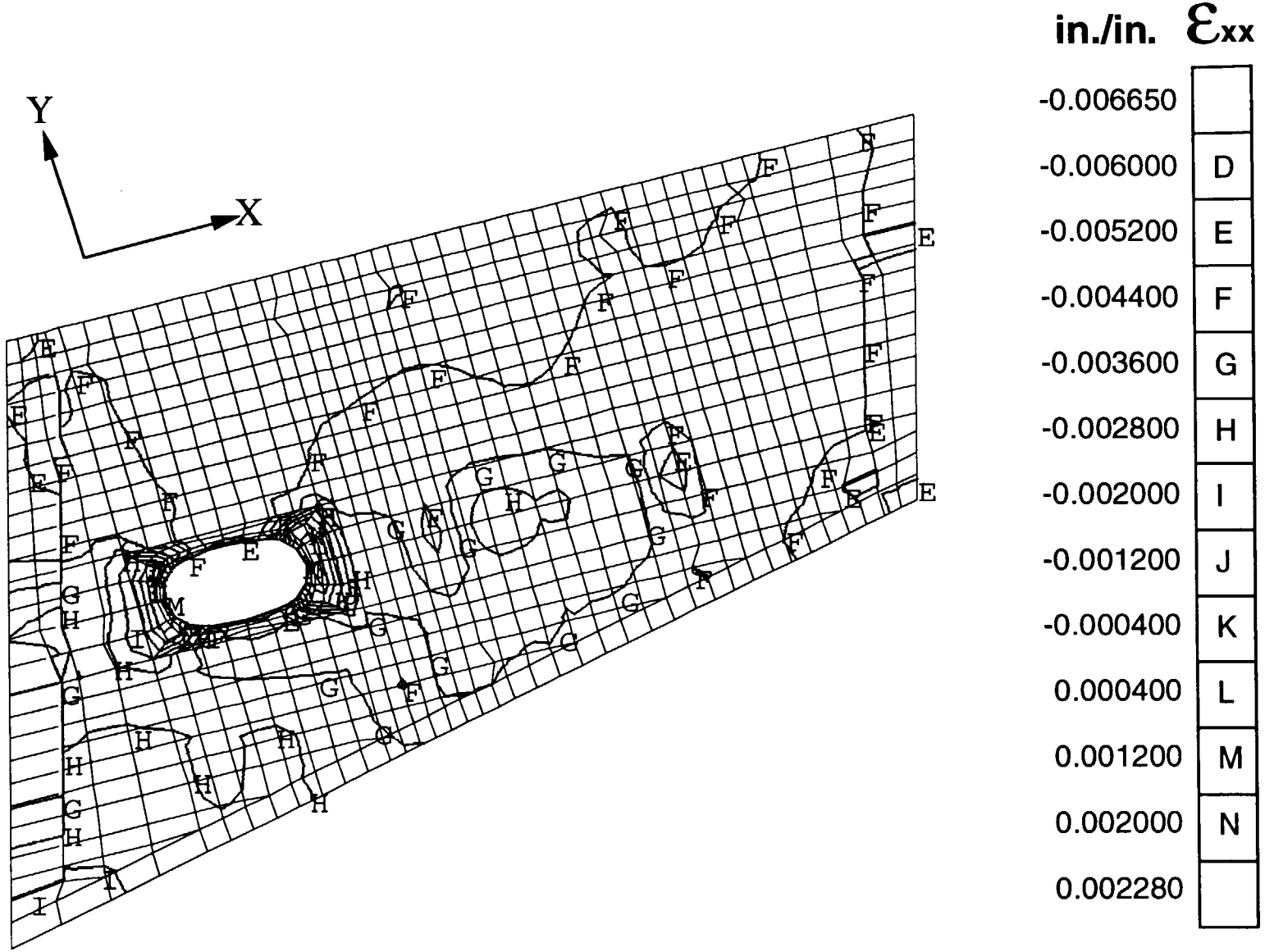

Figure 19. Predicted longitudinal strain contours at stiffener-side surface of upper cover due to 166,000 lb. tip load.

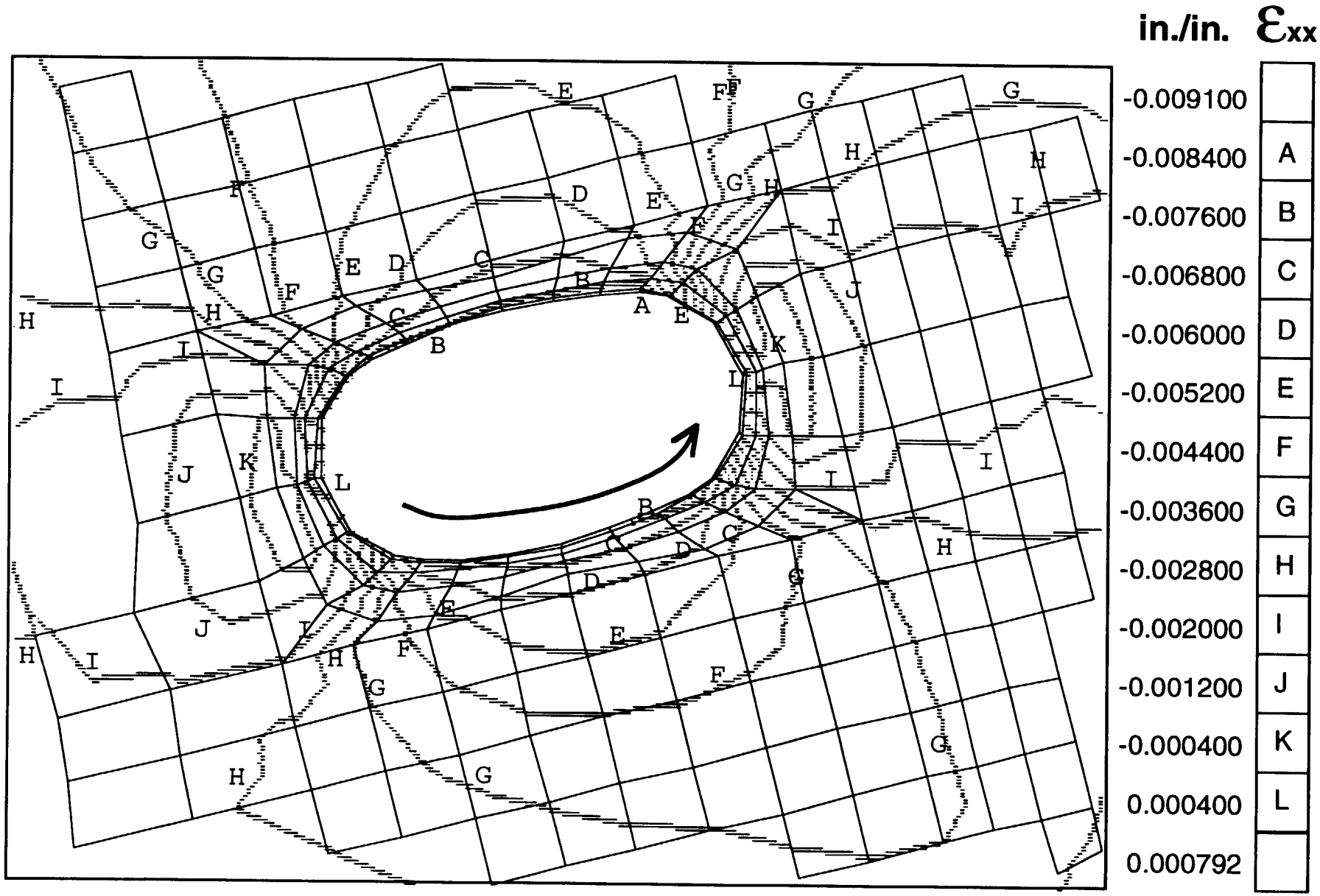

Figure 20. Predicted contours of strain circumferential to hole at skin-side surface of upper cover due to 166,000 lb. tip load.

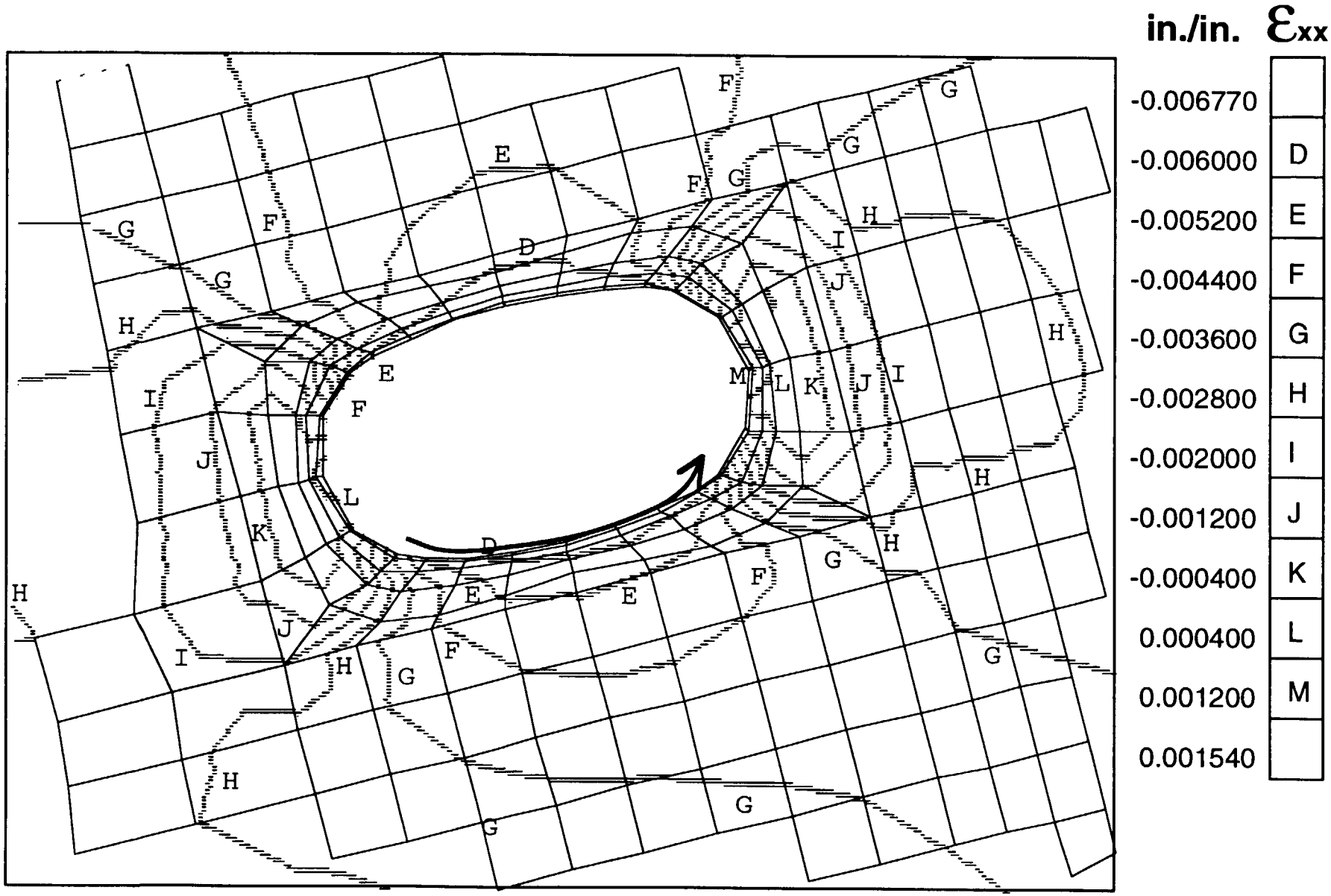

Figure 21. Predicted contours of strain circumferential to hole at mid-surface of upper cover due to 166,000 lb. tip load.

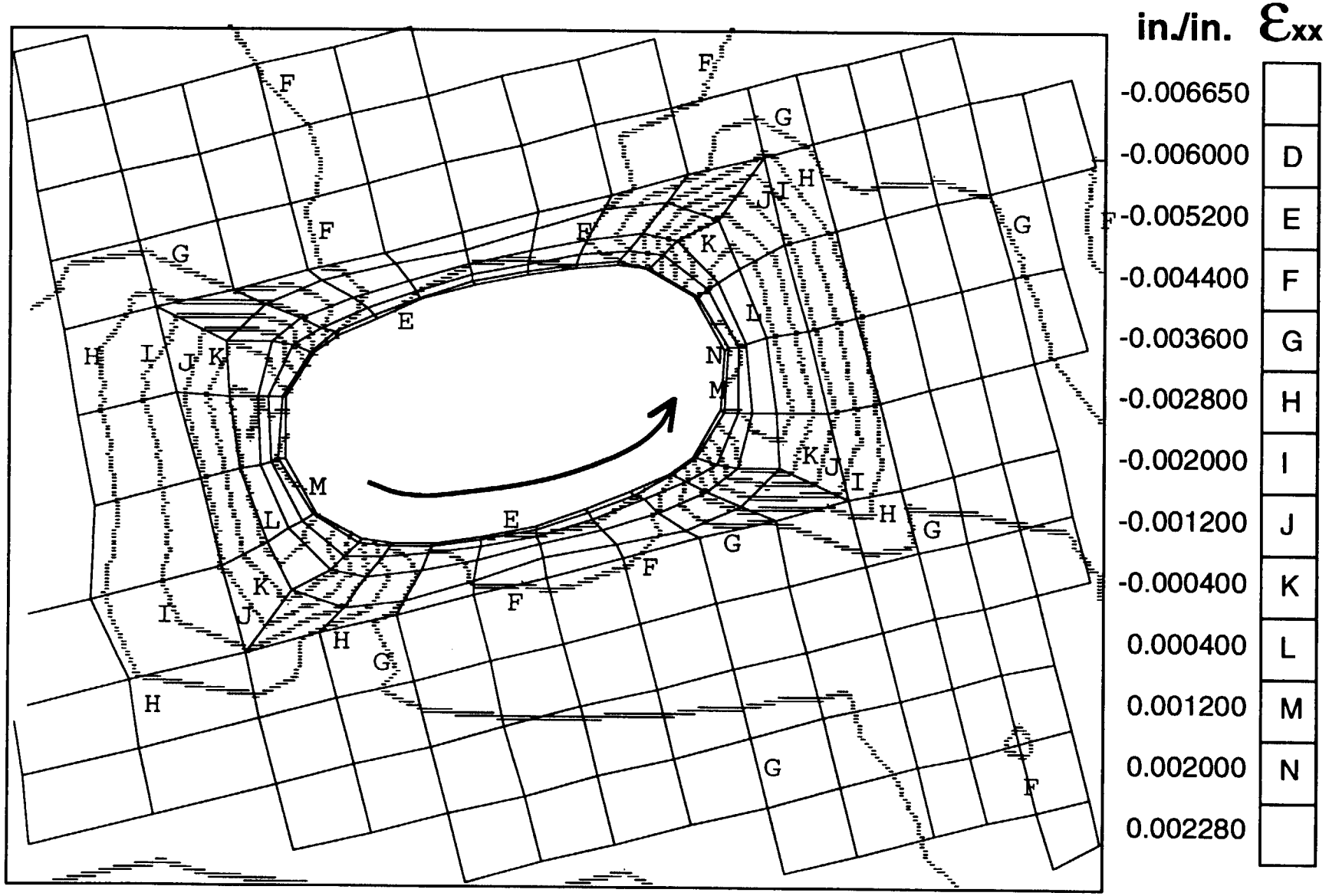

Figure 22. Predicted contours of strain circumferential to hole at stiffener-side surface of upper cover due to 166,000 lb. tip load.

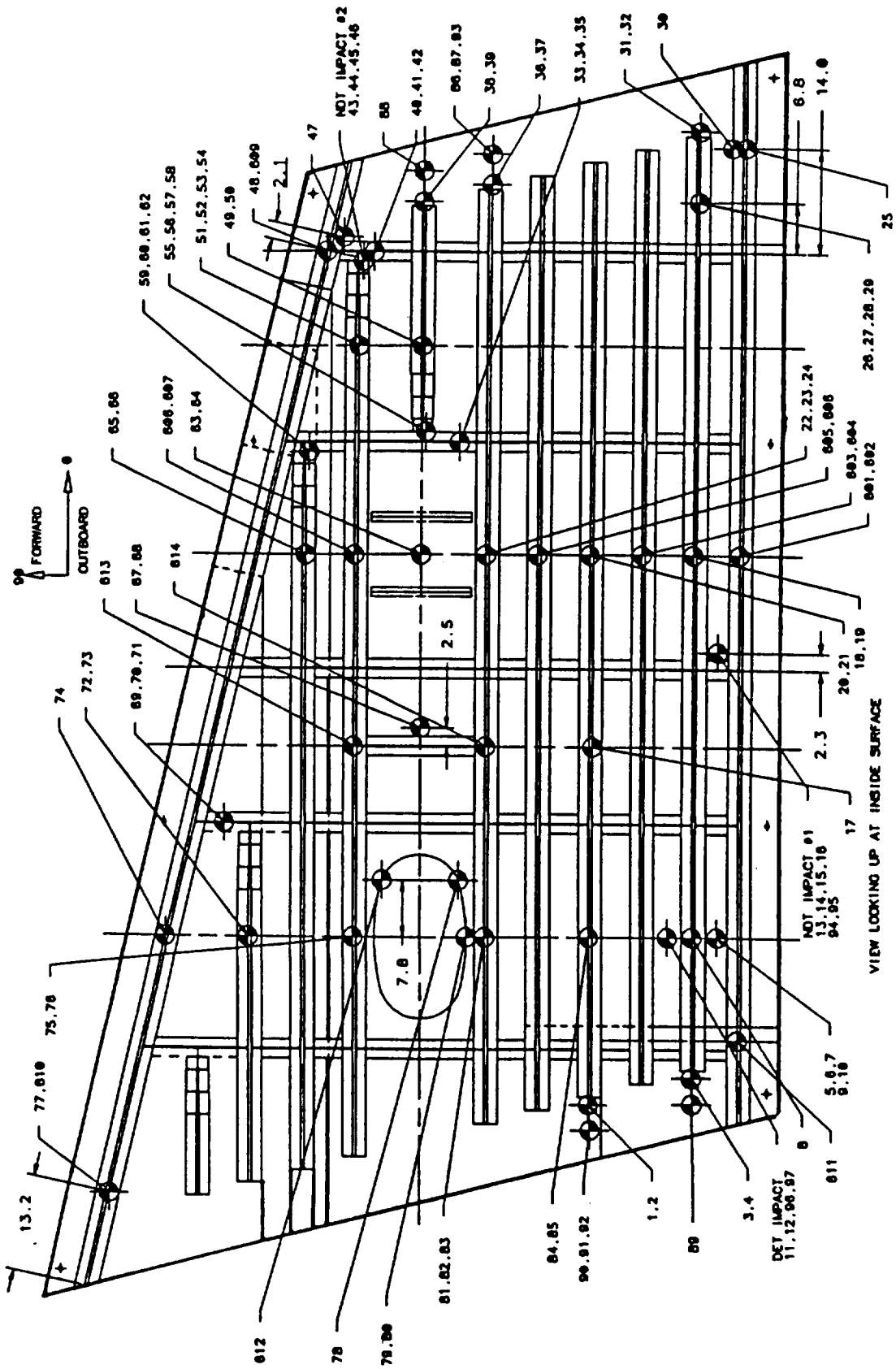

Figure 23. Upper skin strain gage locations.

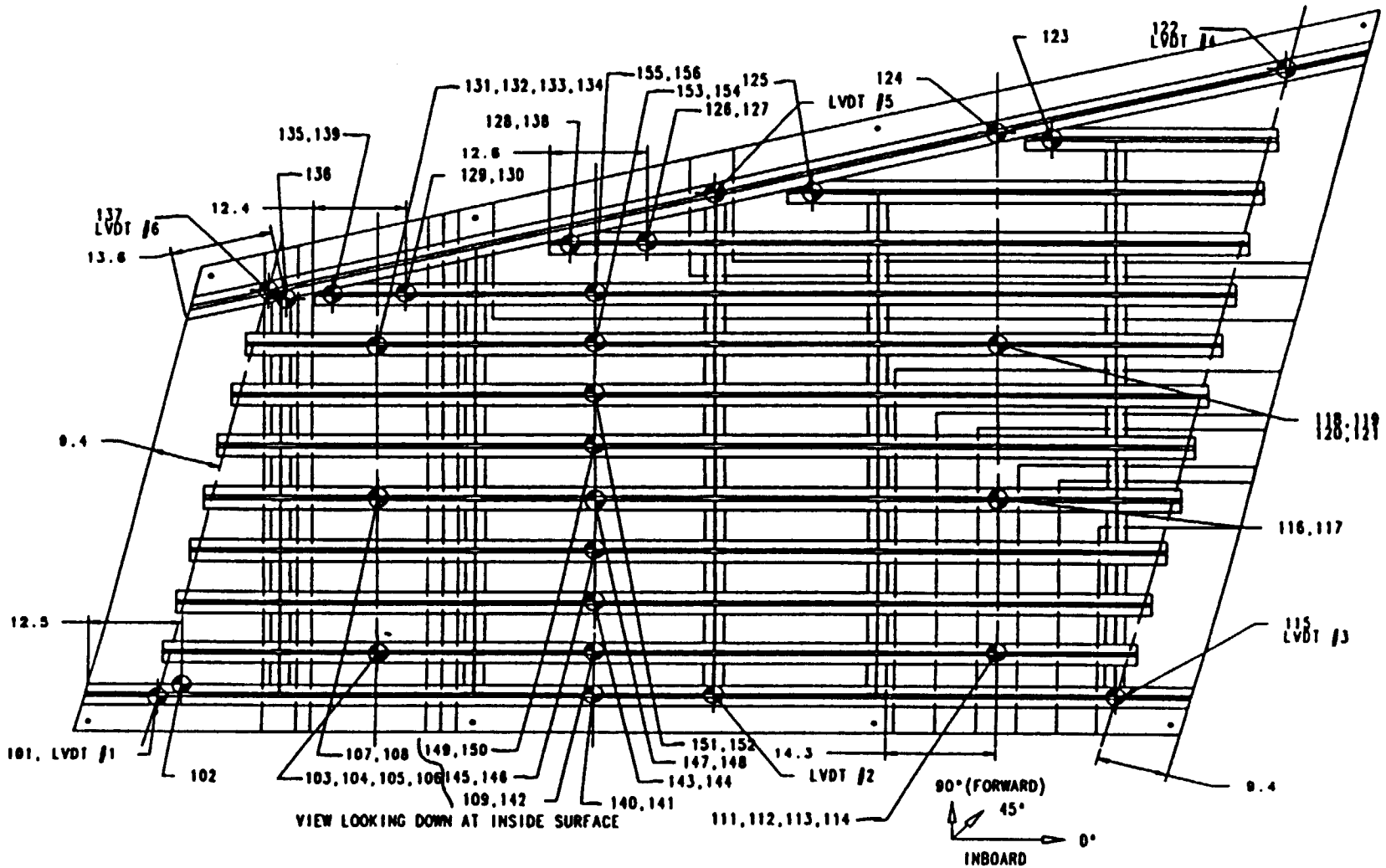

Figure 24. Lower skin strain gage locations.

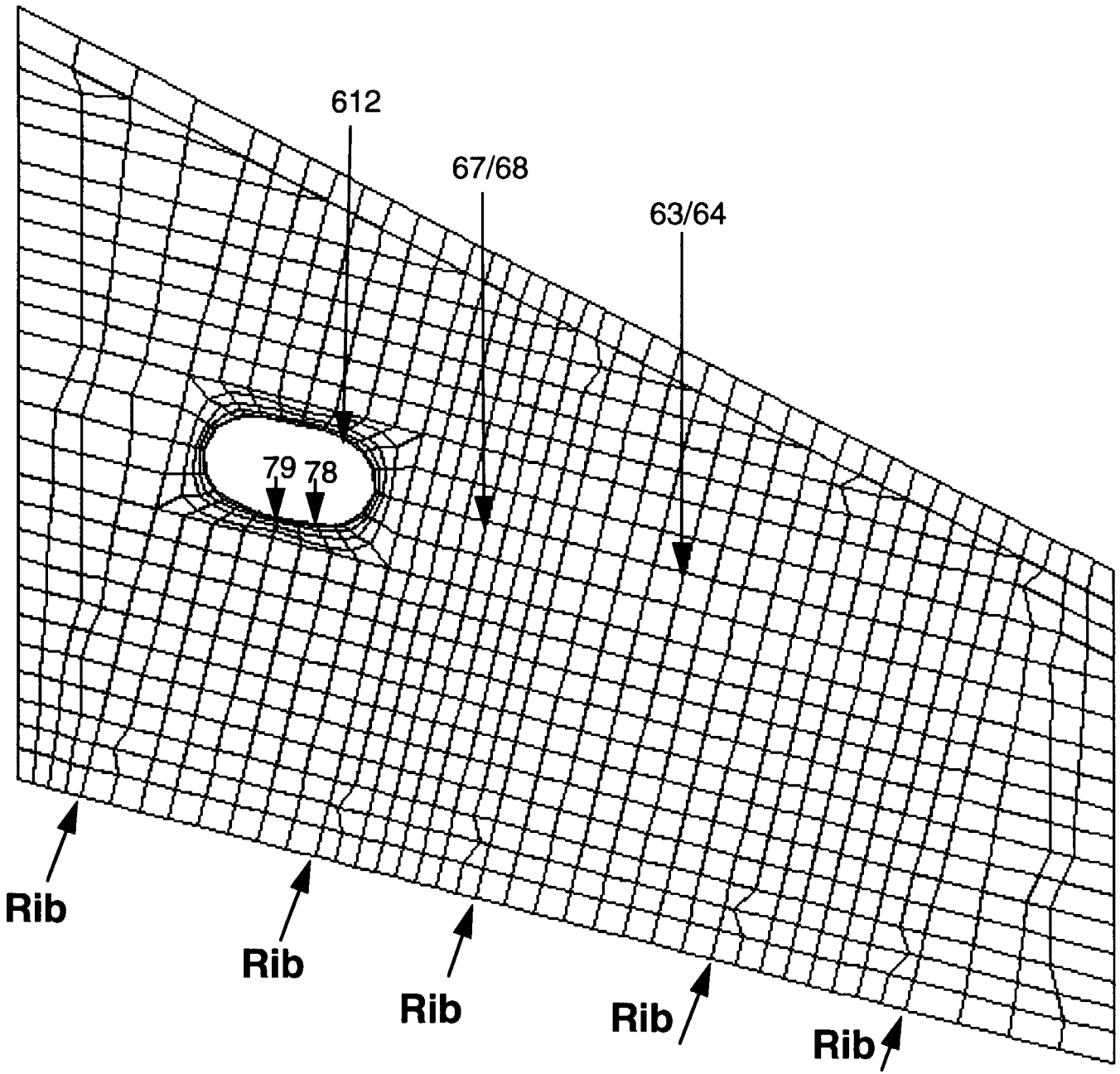

Figure 25. Selected strain gage locations on top cover.

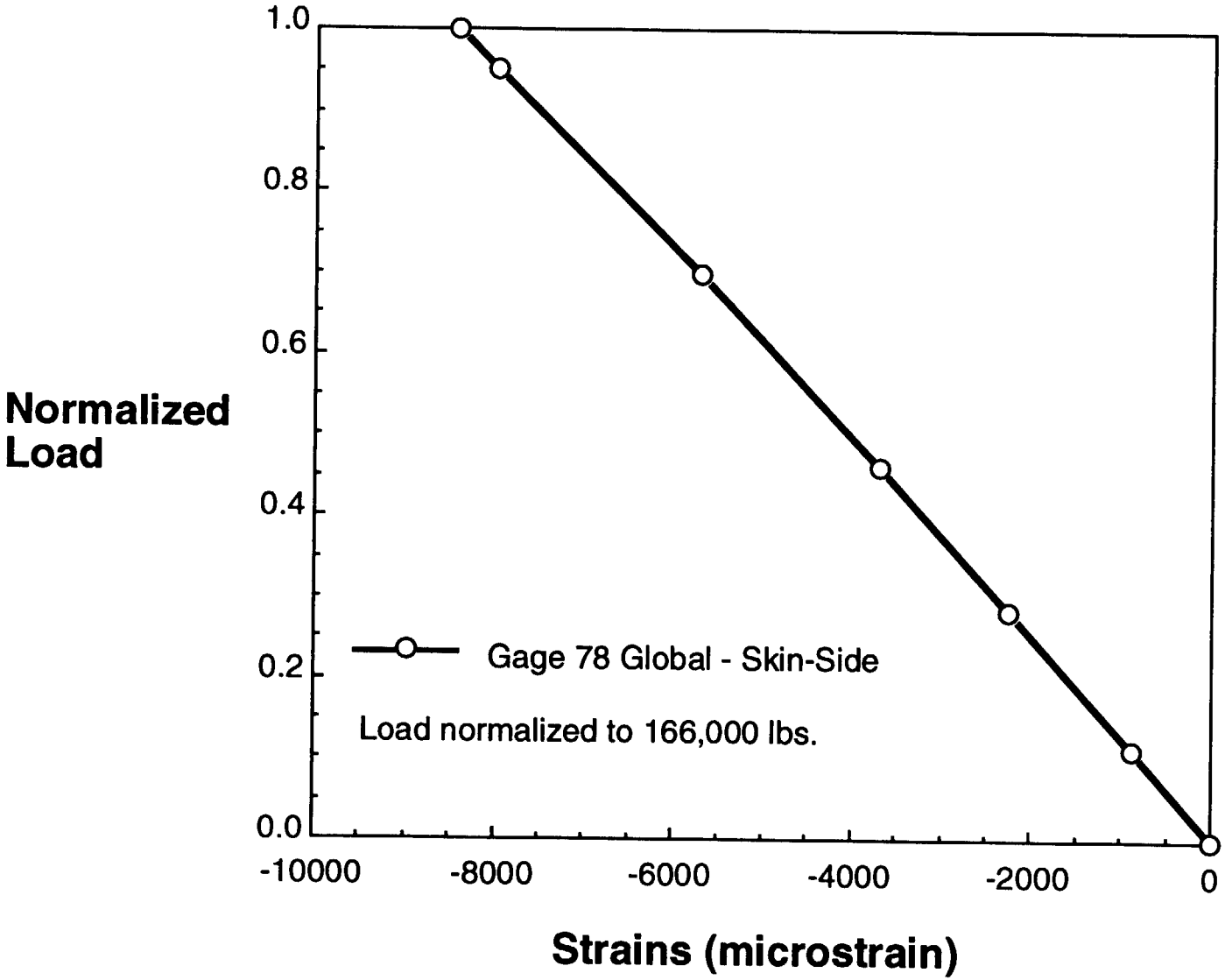

Figure 26. Predicted strains at locations of gage 78.

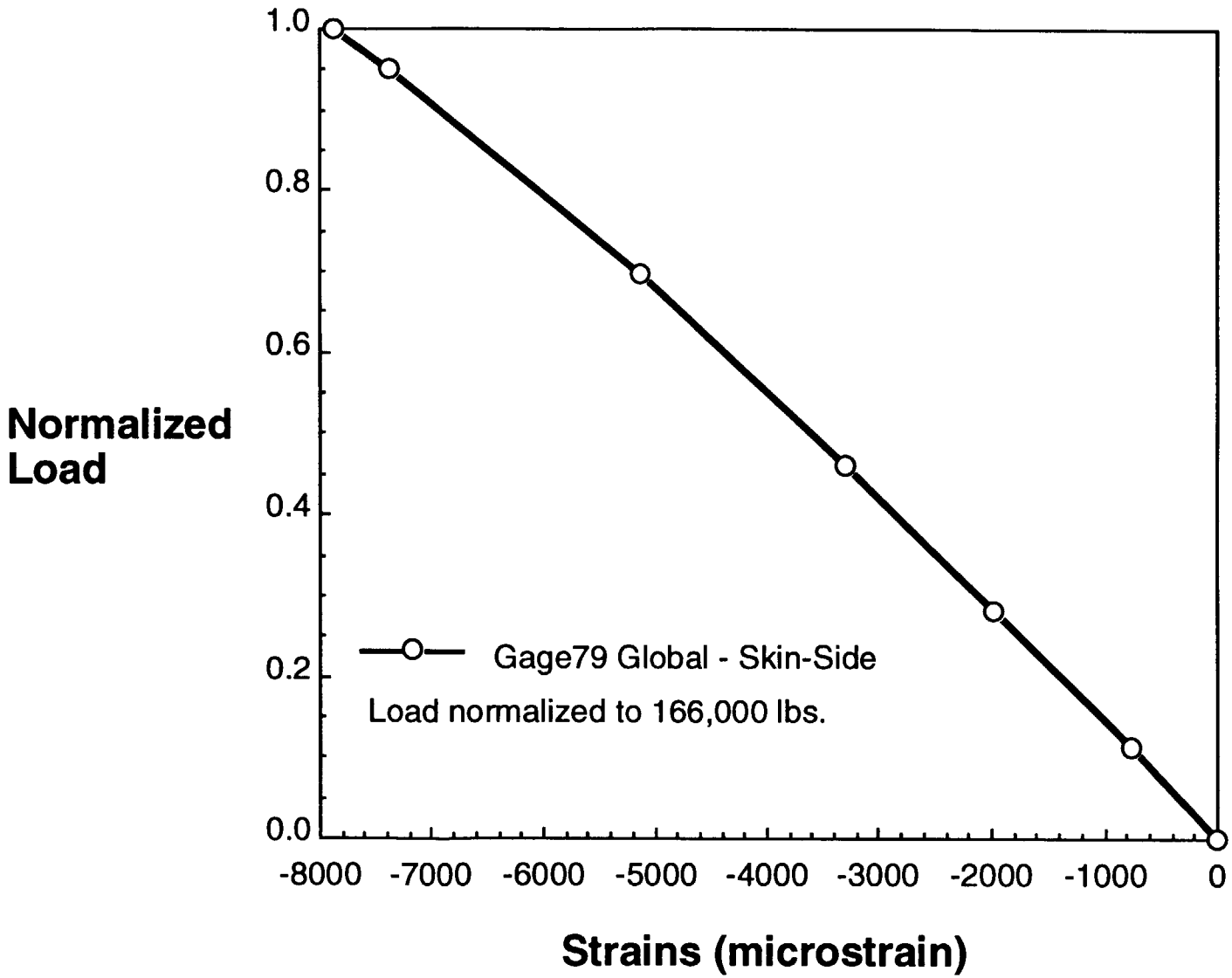

Figure 27. Predicted strains at location of gage 79.

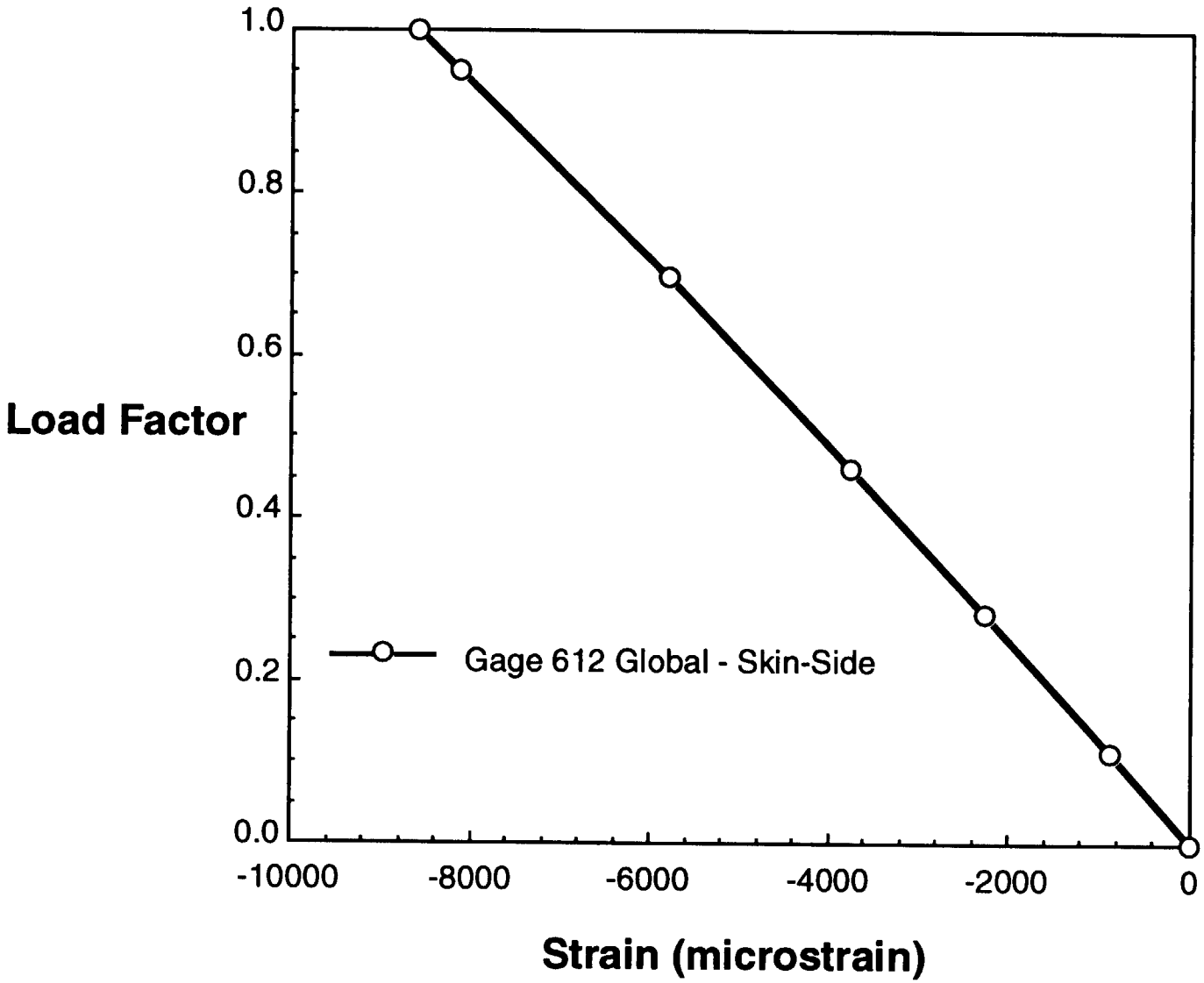

Figure 28. Strains in gages 612.

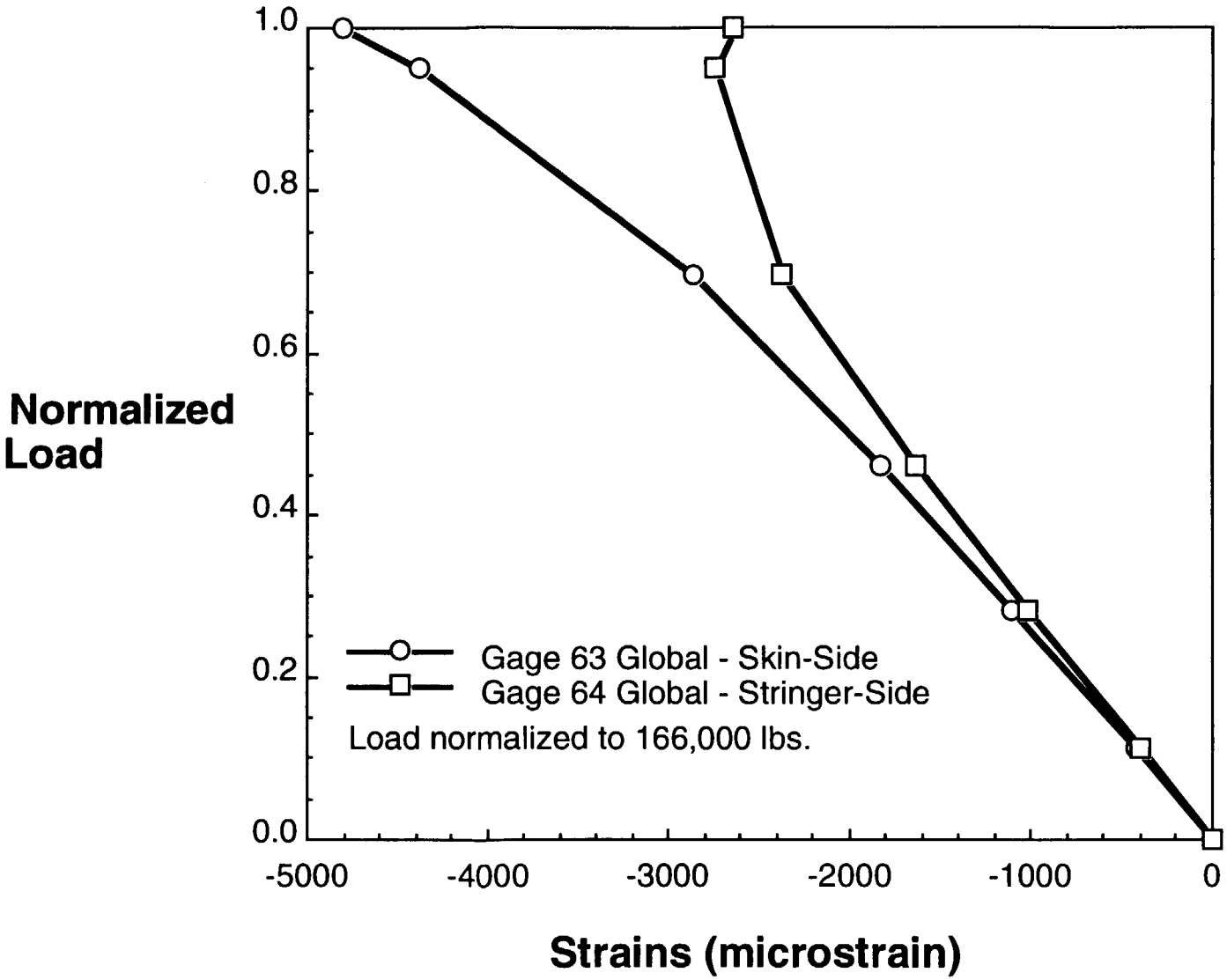

Figure 29. Predicted strains at locations of gages 63 and 64.

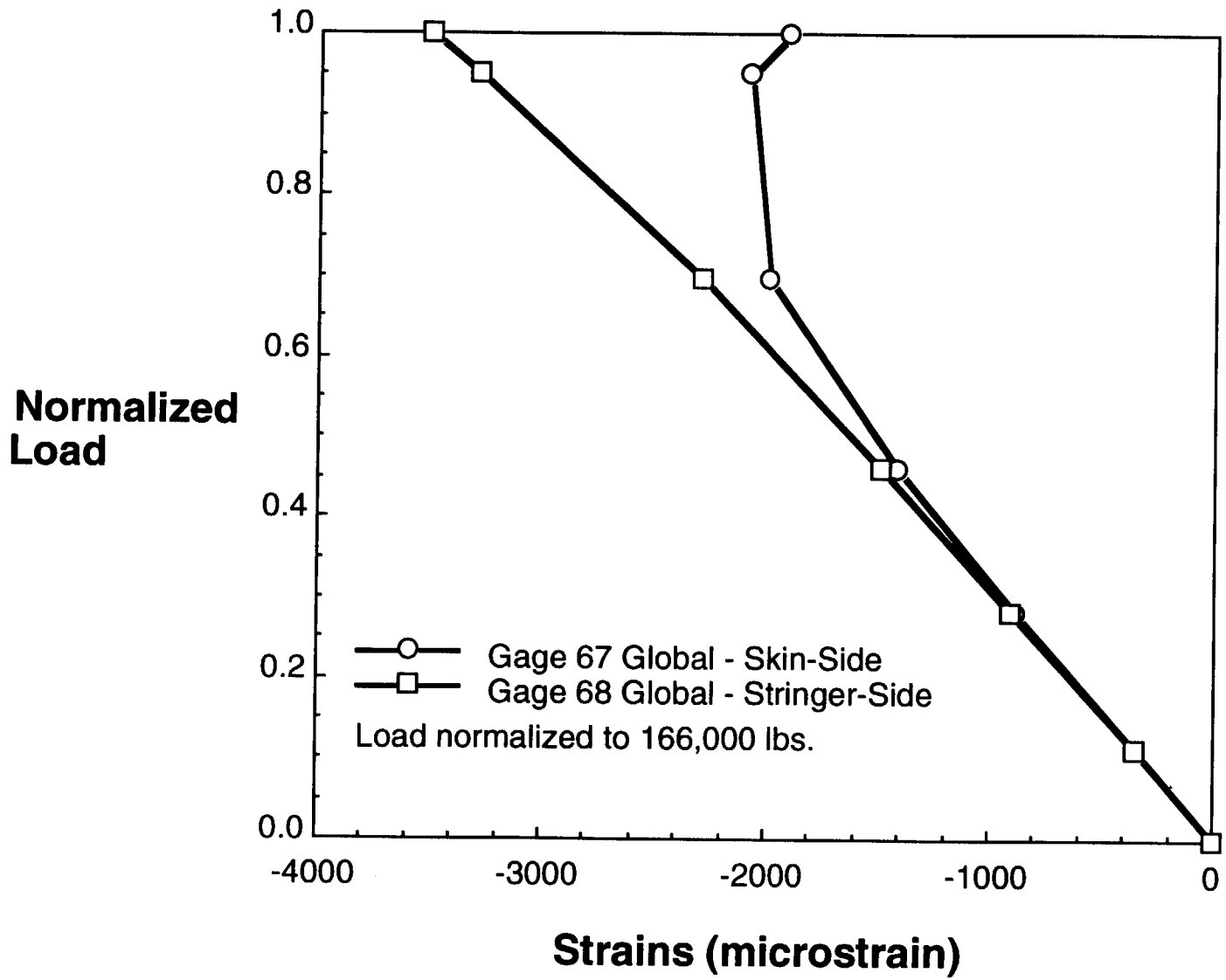

Figure 30. Predicted strains at the locations of gages 67 and 68.

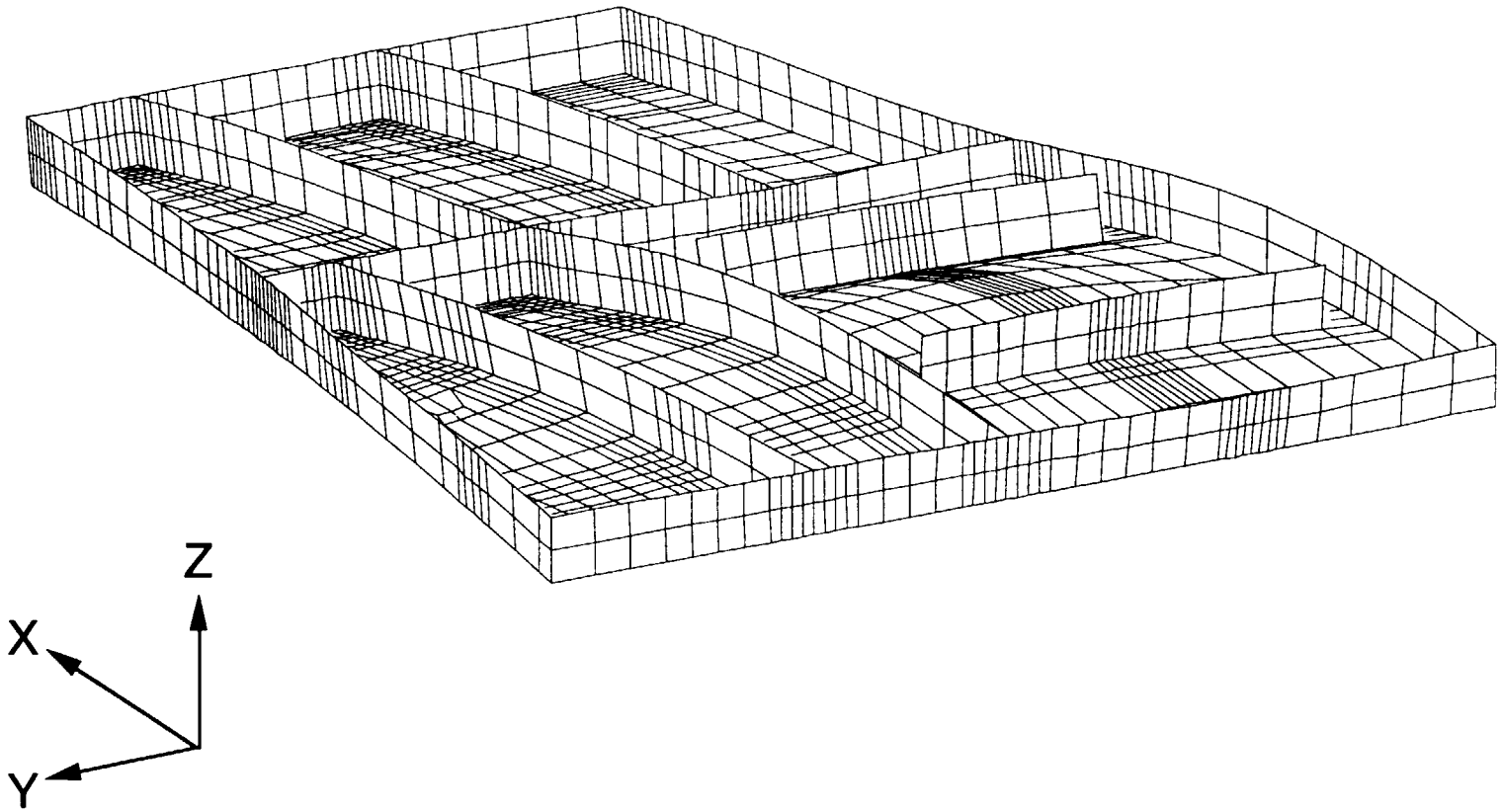

Figure 31. Predicted deformed shape of local model due to 166,000 lb. tip load.

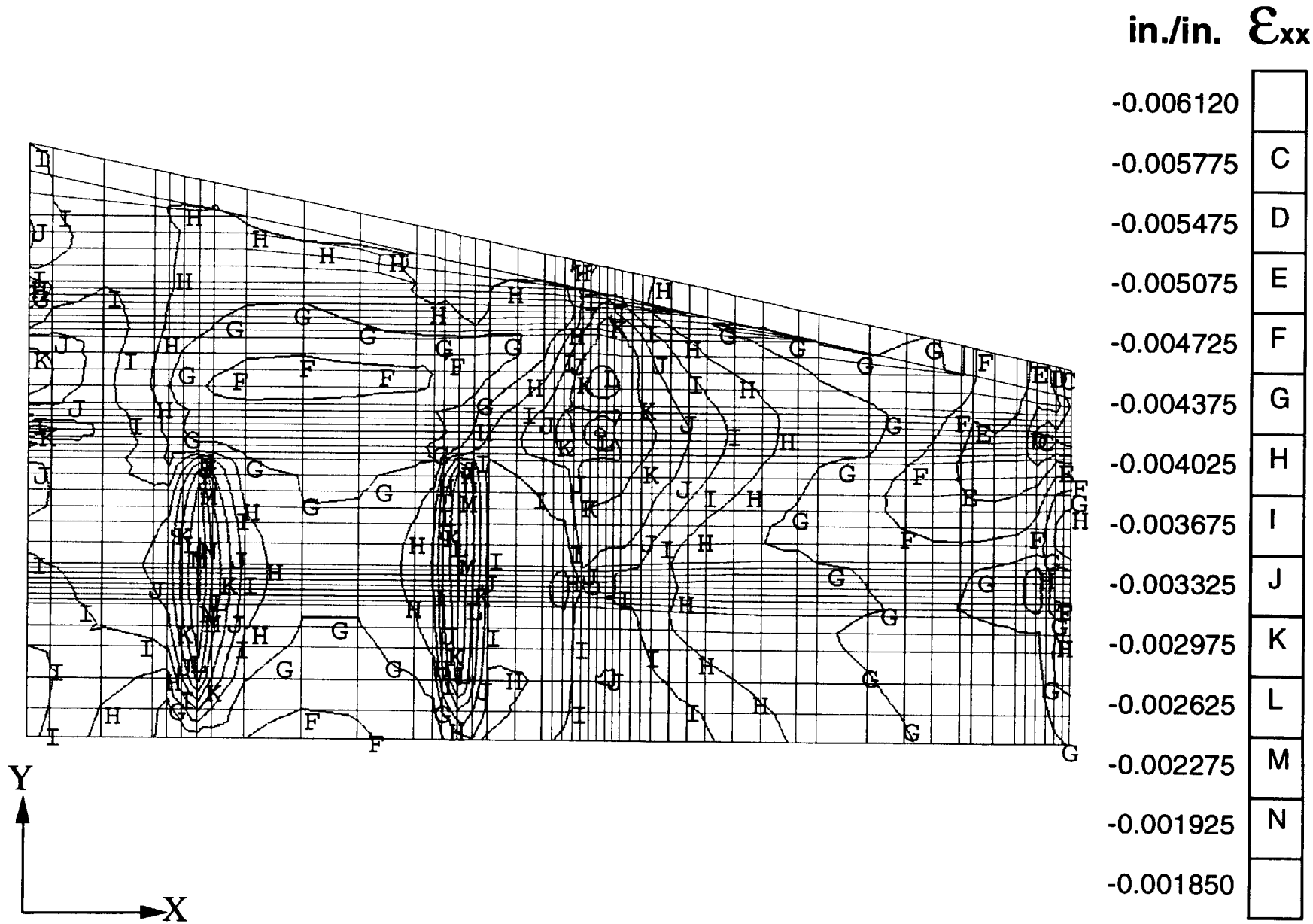

Figure 32. Predicted longitudinal strain contours at skin-side surface of upper cover due to 166,000 lb. tip load.

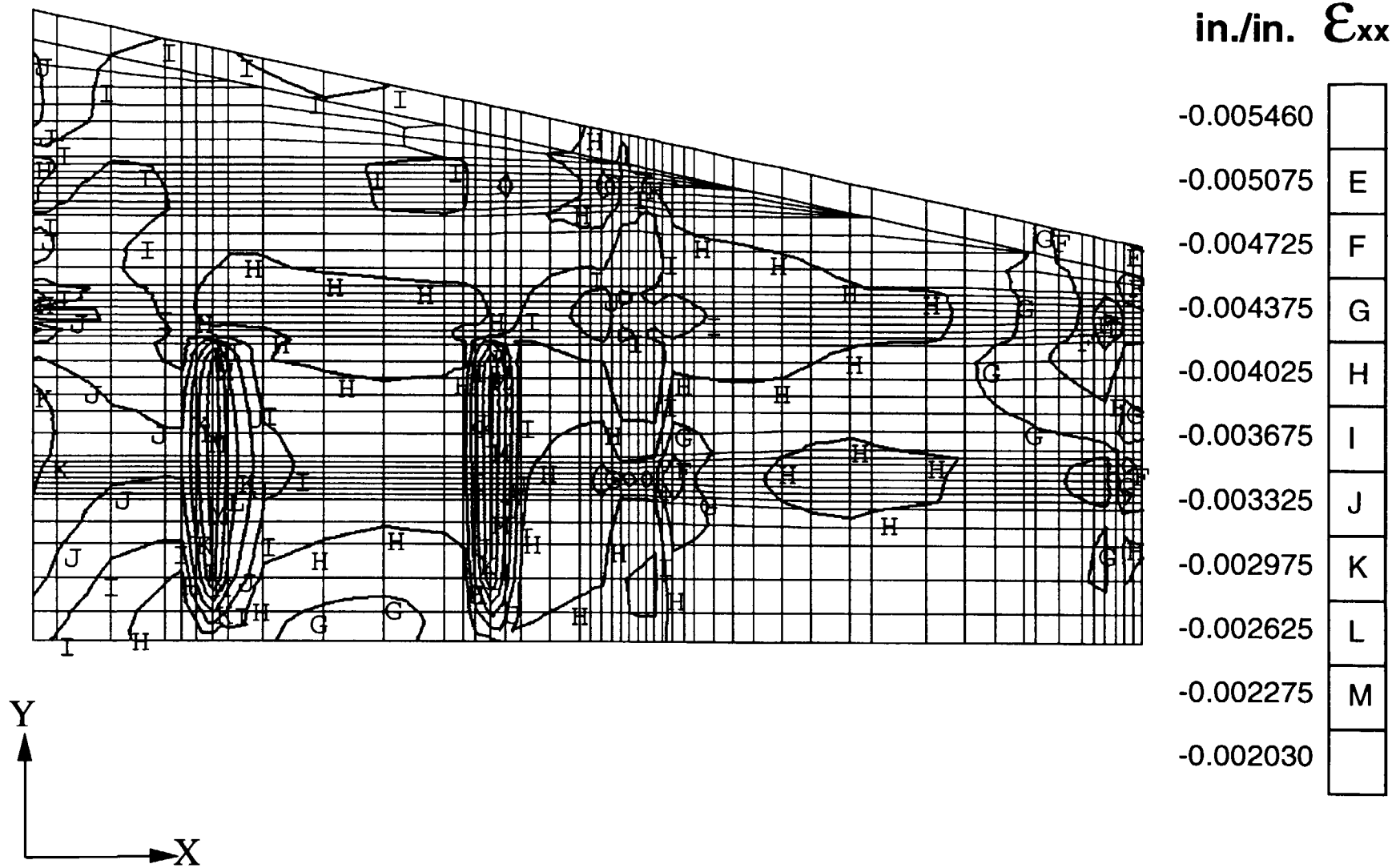

Figure 33. Predicted longitudinal strain contours at mid-surface of upper cover due to 166,000 lb. tip load.

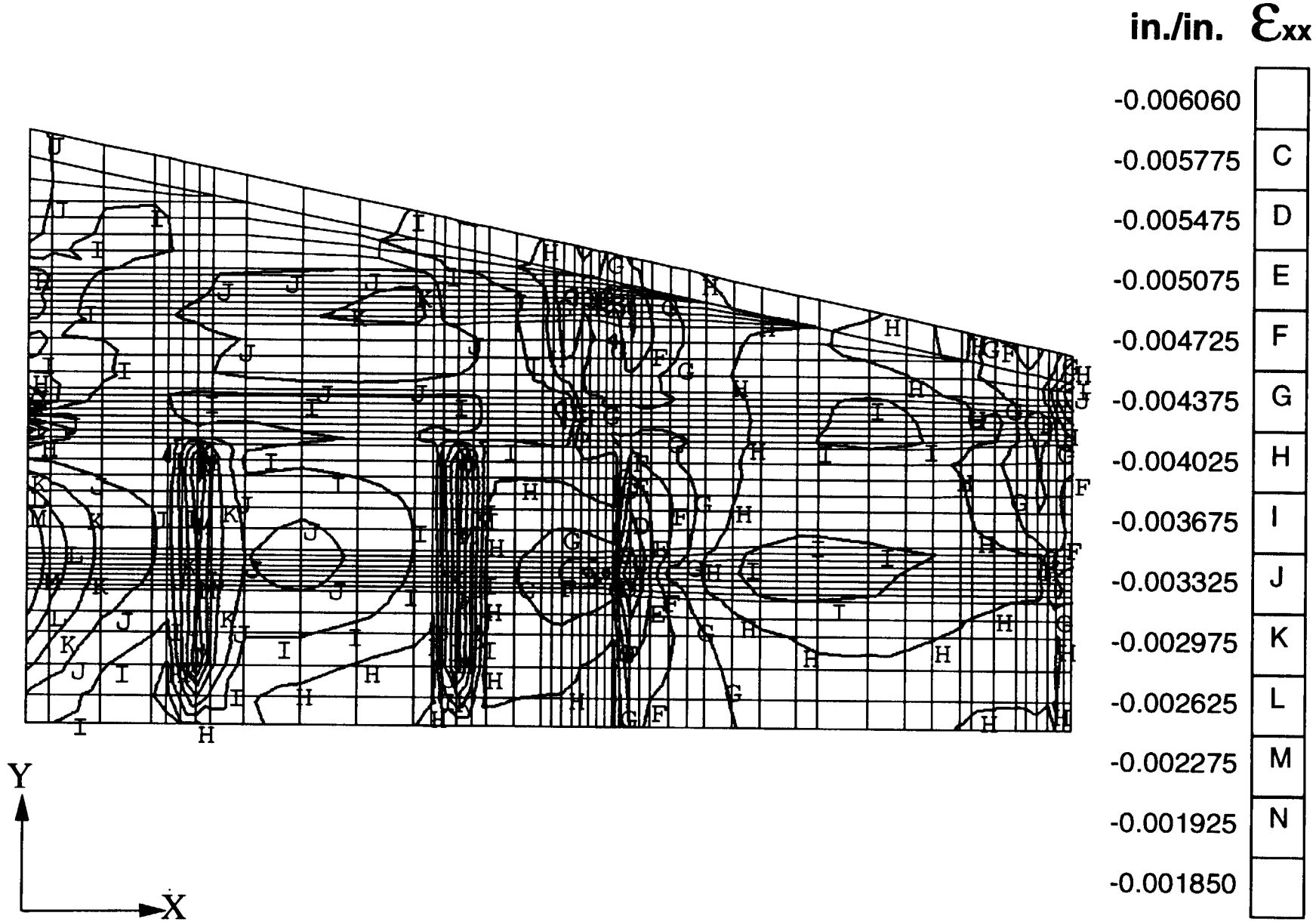

Figure 34. Predicted longitudinal strain contours at stiffener-side surface of upper cover due to 166,000 lb. tip load.

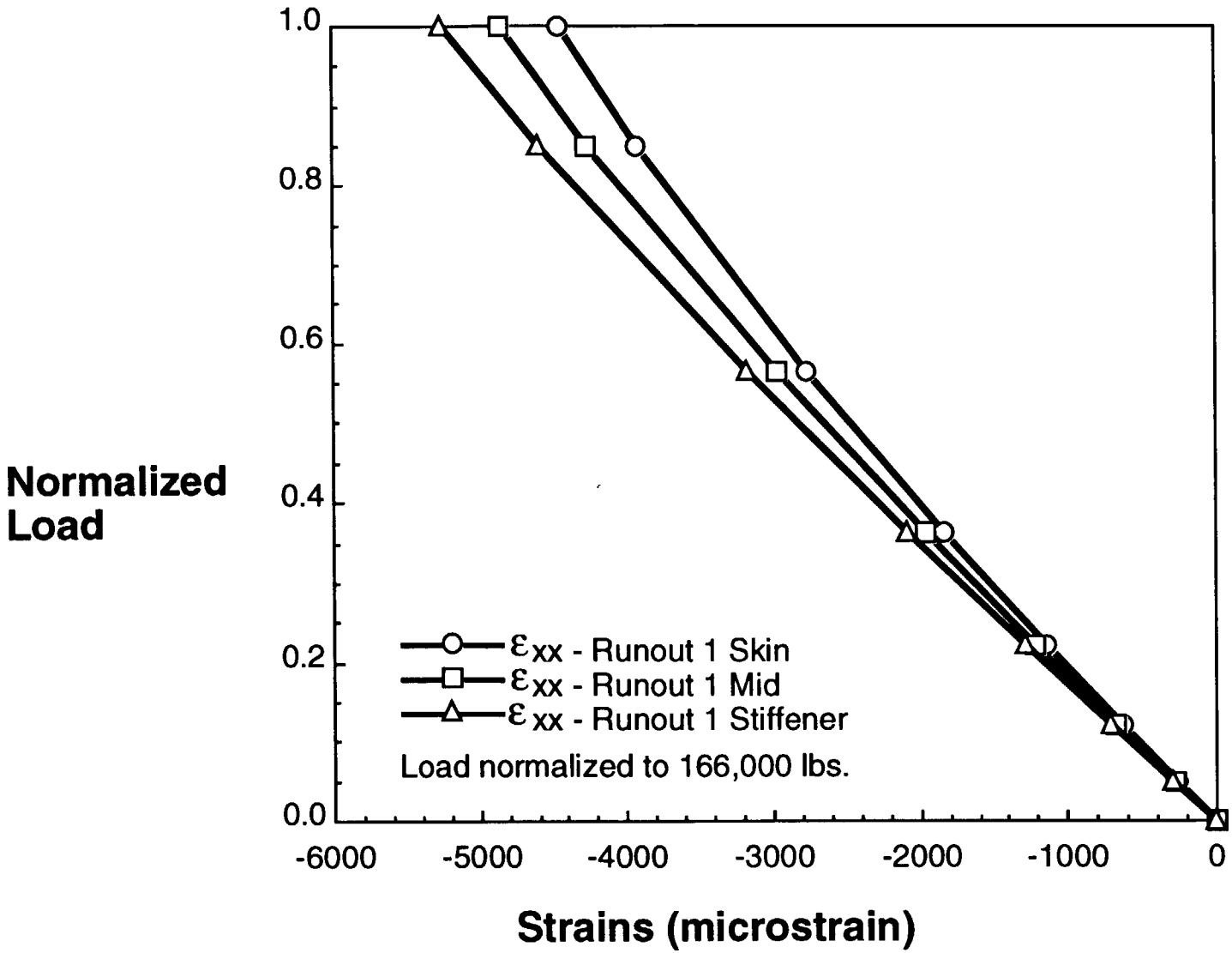

Figure 35. Predicted longitudinal strains for gage at runout 1.

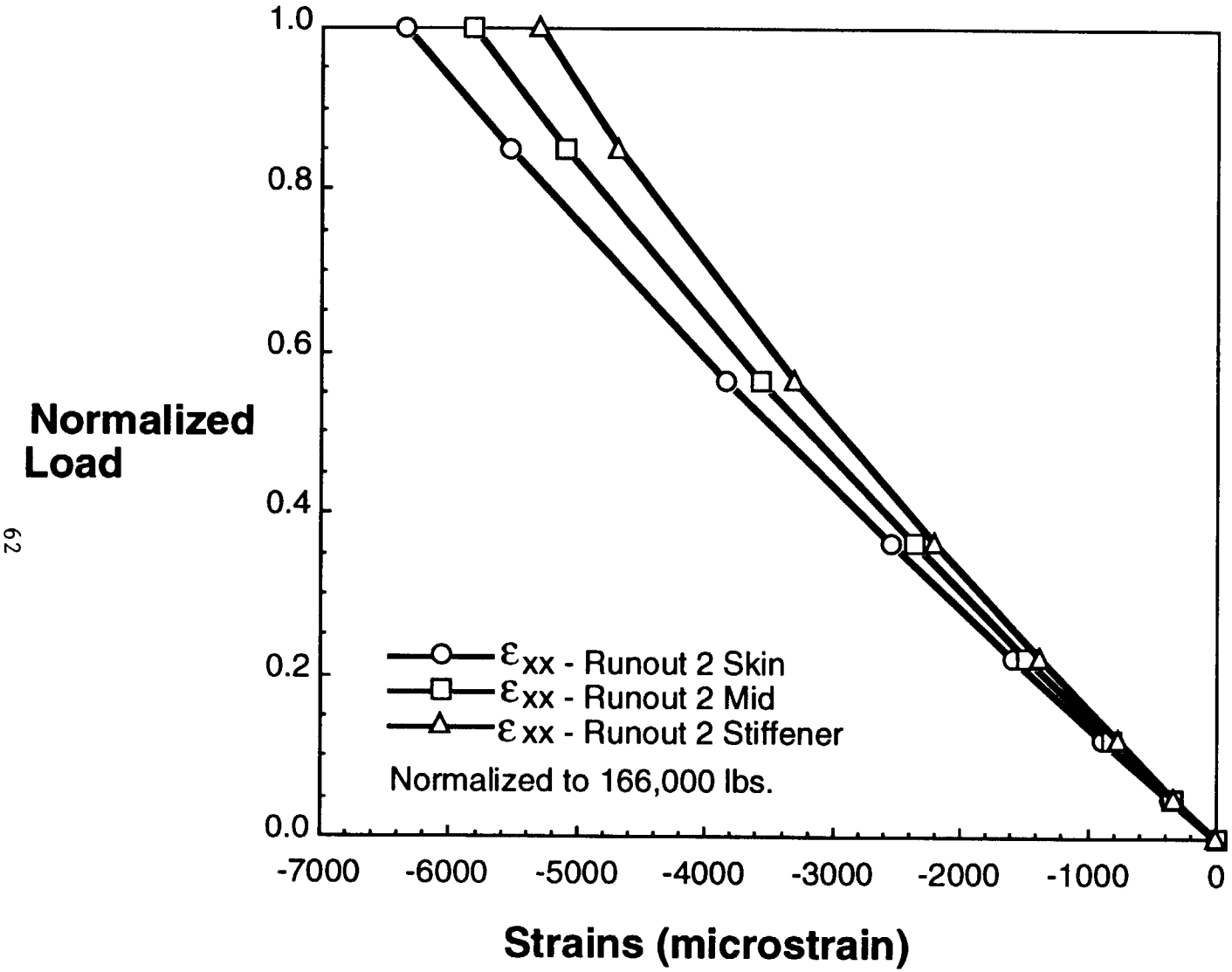

Figure 36. Predicted longitudinal strains for gage at runout 2.

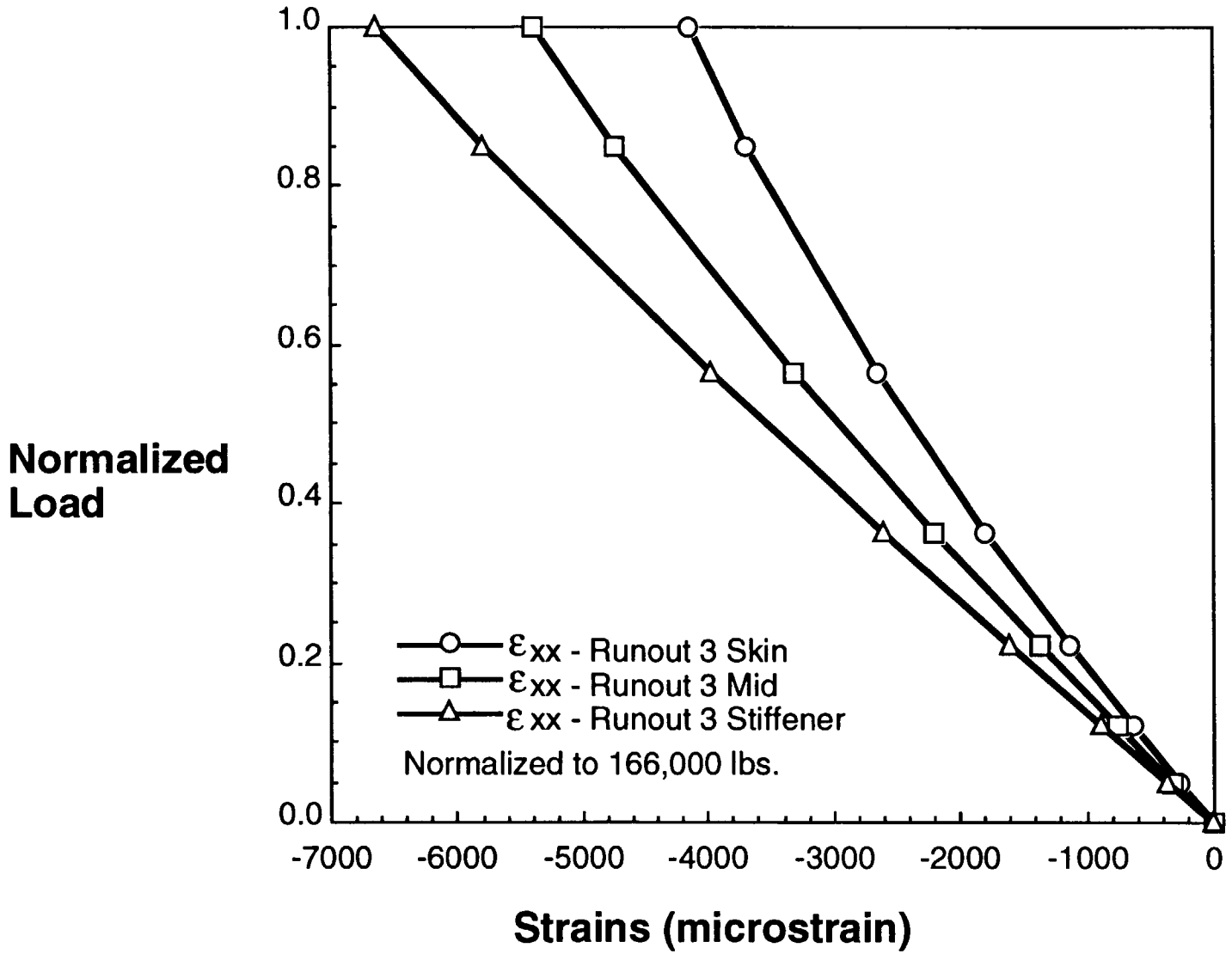

Figure 37. Predicted longitudinal strains for gage at runout 3.

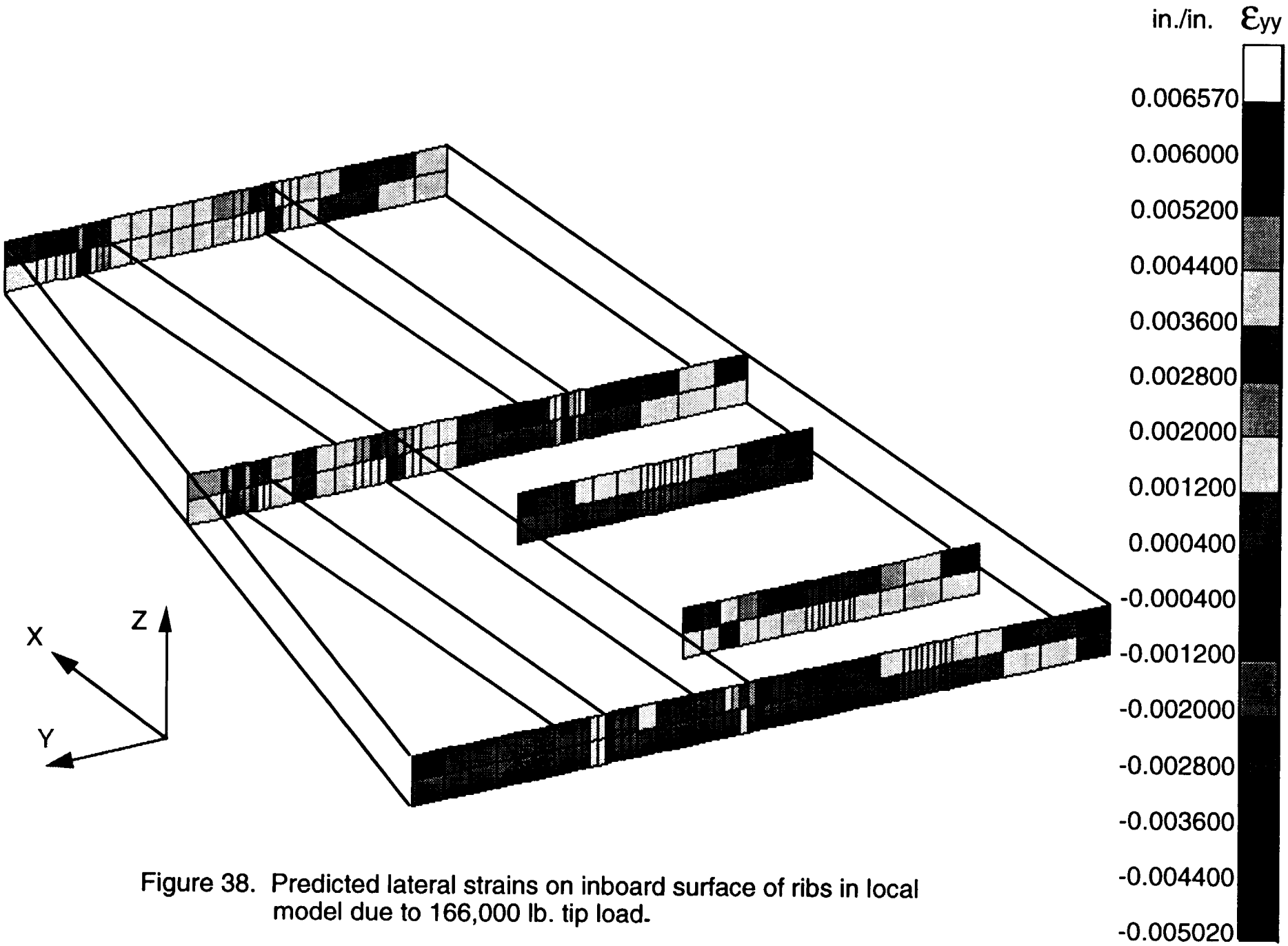

Figure 38. Predicted lateral strains on inboard surface of ribs in local model due to 166,000 lb. tip load.

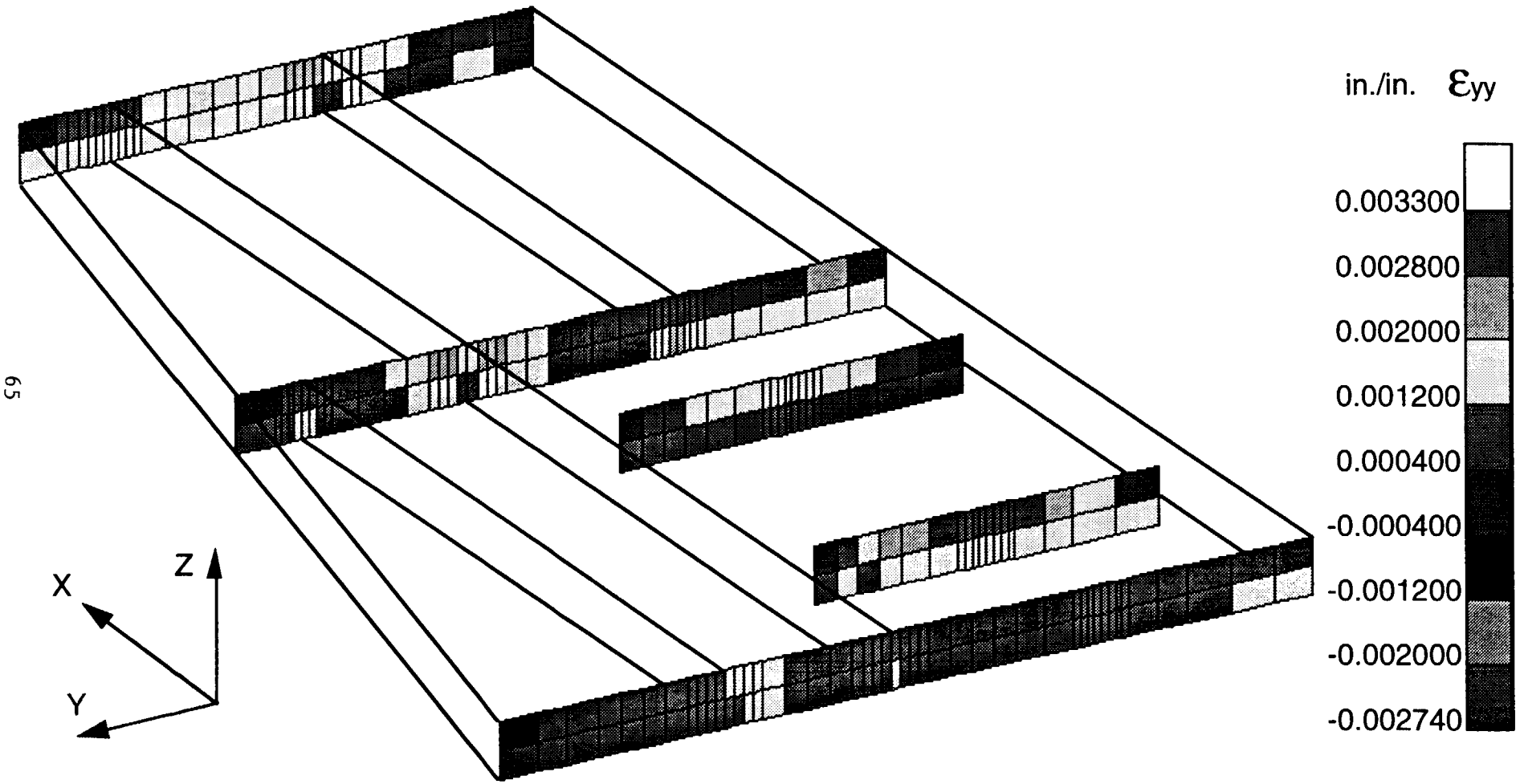

Figure 39. Predicted lateral strains on mid-surface of the ribs in local model due to 166,000 lb. tip load.

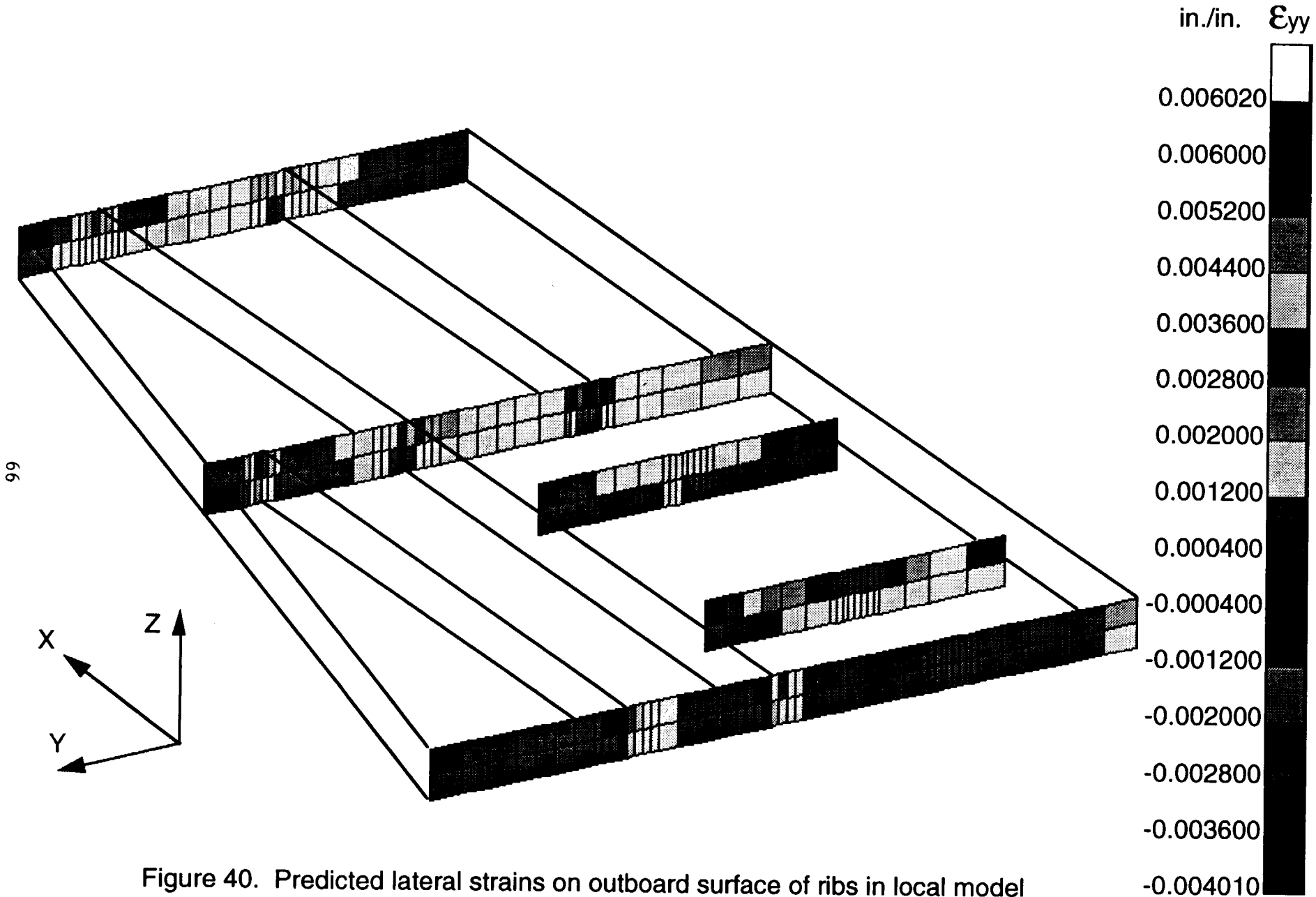

Figure 40. Predicted lateral strains on outboard surface of ribs in local model due to 166,000 lb. tip load.

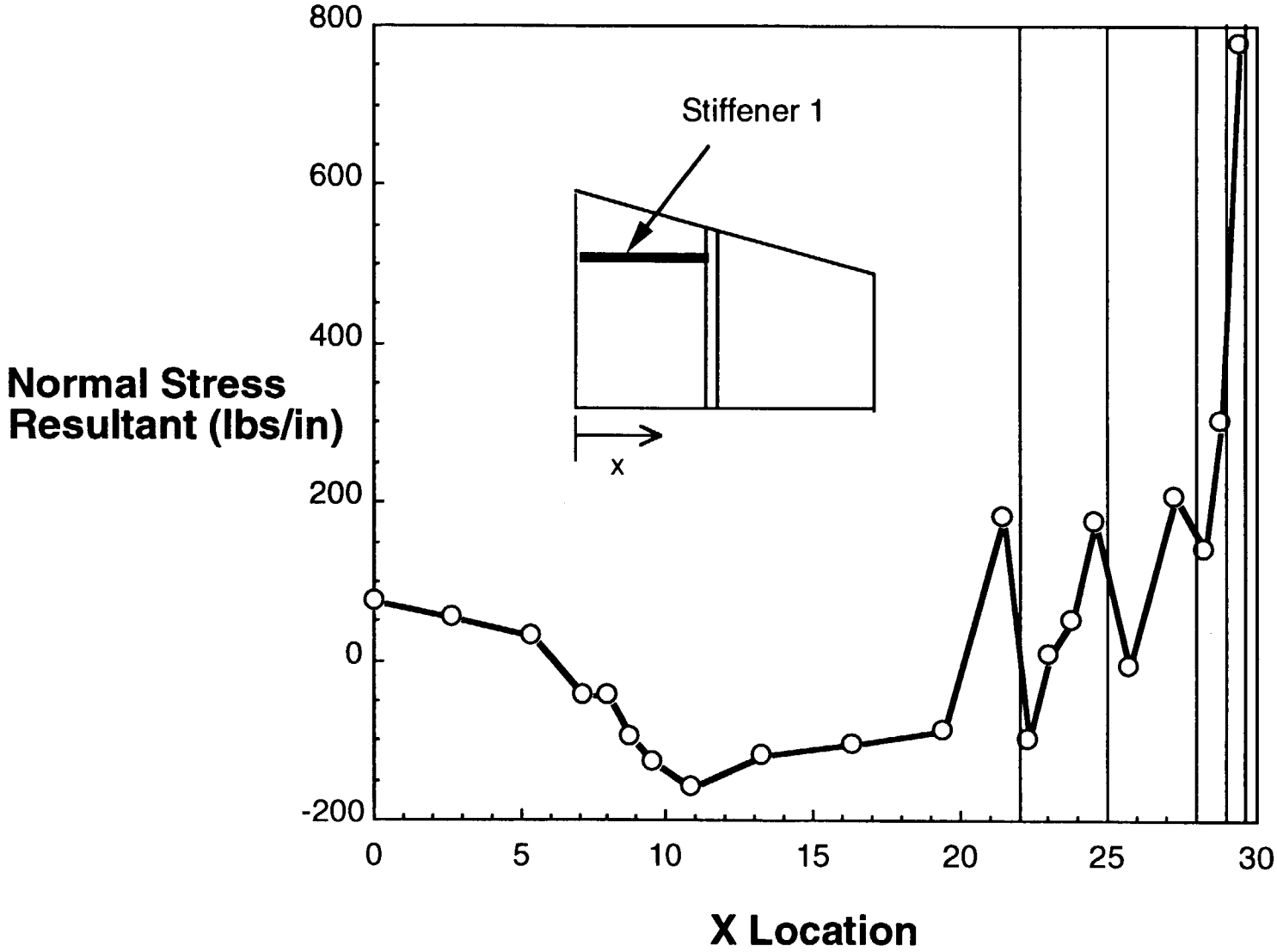

Figure 41. Predicted normal stress resultant (separation load) between stiffener 1 and skin in upper cover.

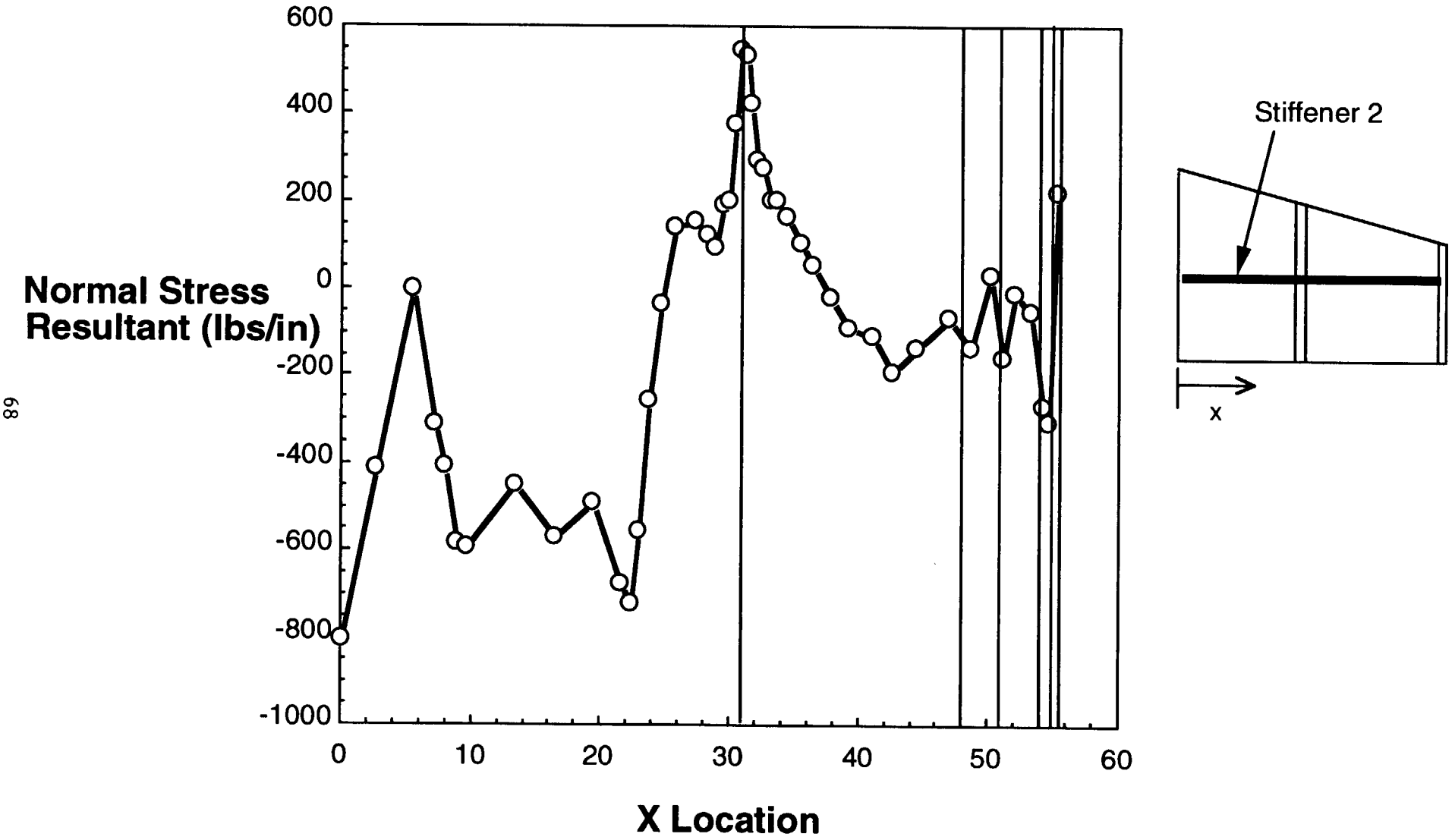

Figure 42. Predicted normal stress resultant (separation load) between stiffener 2 and skin of upper cover .

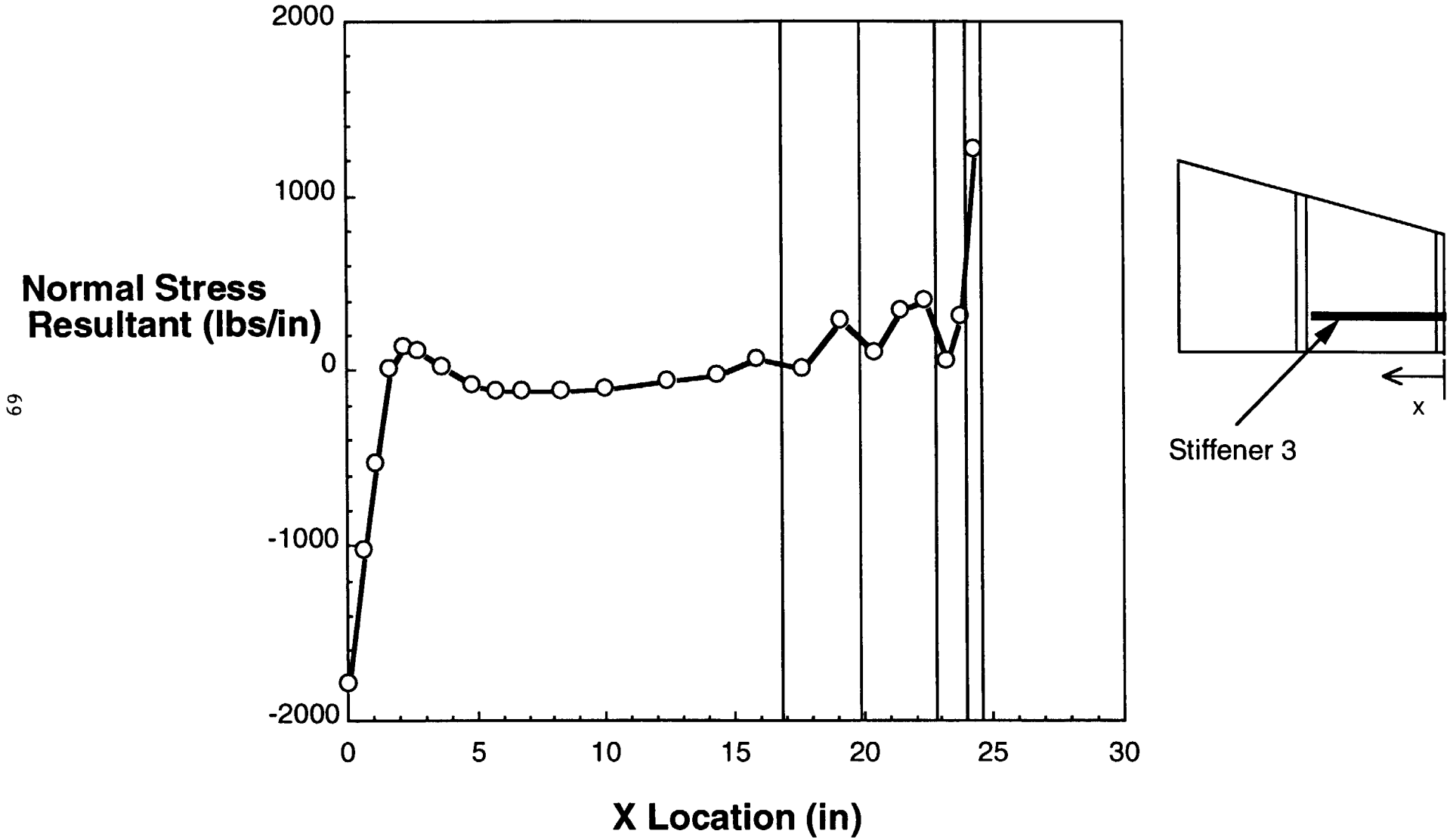

Figure 43. Predicted normal stress resultant (separation load) between stiffener 3 and the skin of the upper cover.

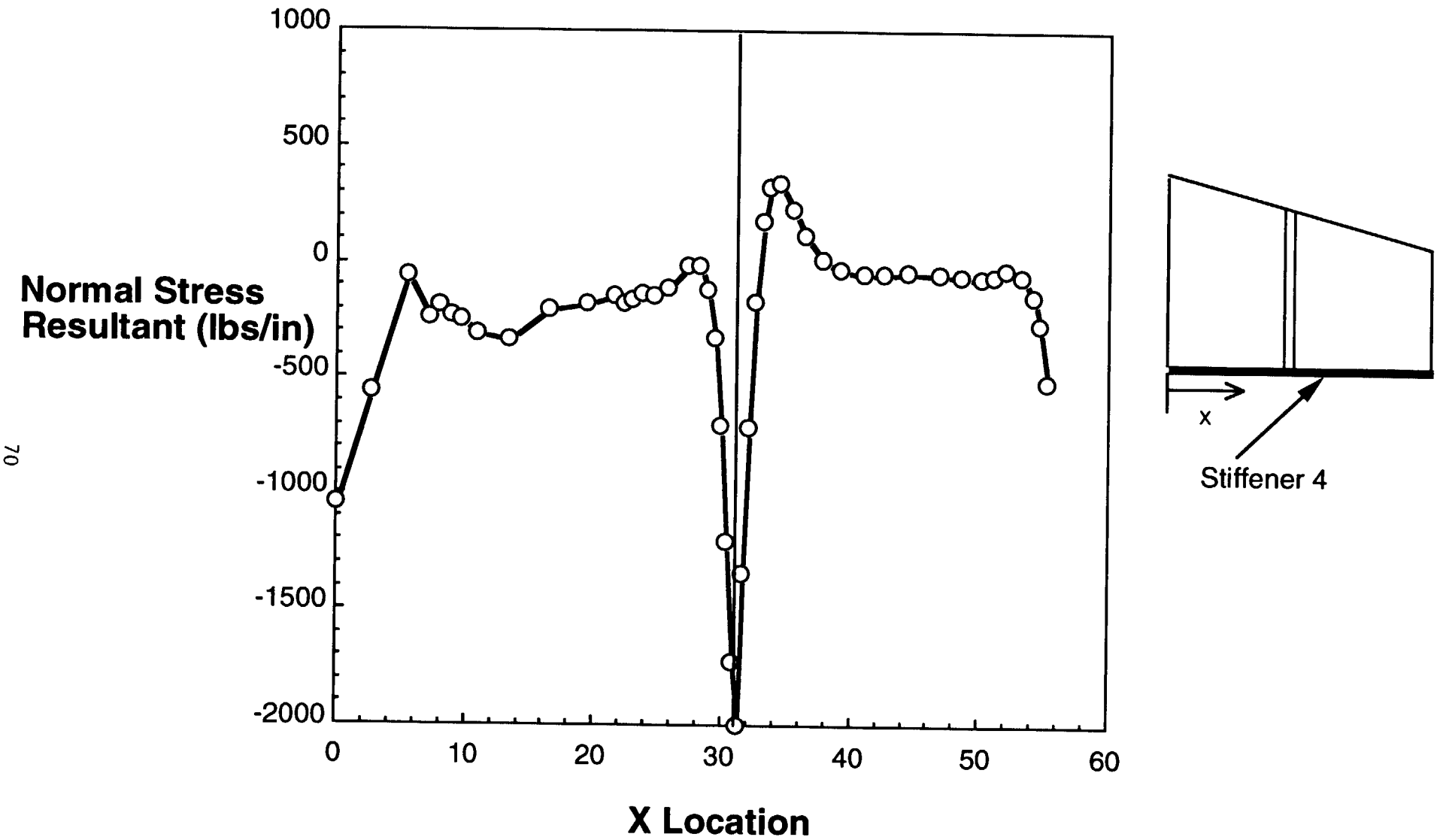

Figure 44. Predicted normal stress resultant (separation load) between stiffener 4 and the skin of the upper cover.

REPORT DOCUMENTATION PAGE

Form Approved
OMB No. 0704-0188

1. AGENCY USE ONLY (*Leave blank*)	2. REPORT DATE	3. REPORT TYPE AND DATES COVERED
	March 1996	Technical Memorandum

4. TITLE AND SUBTITLE
Global and Local Stress Analyses of McDonnell Douglas Stitched/RFI Composite Wing Stub Box

5. FUNDING NUMBERS
510-02-12-04

6. AUTHOR(S)
John T. Wang

7. PERFORMING ORGANIZATION NAME(S) AND ADDRESS(ES)
NASA Langley Research Center
Hampton, VA 23681-0001

8. PERFORMING ORGANIZATION REPORT NUMBER

9. SPONSORING / MONITORING AGENCY NAME(S) AND ADDRESS(ES)
National Aeronautics and Space Administration
Washington, DC 20546-0001

10. SPONSORING / MONITORING AGENCY REPORT NUMBER
NASA TM-110171

11. SUPPLEMENTARY NOTES

12a. DISTRIBUTION / AVAILABILITY STATEMENT
Unclassified - Unlimited
Subject Category 39

12b. DISTRIBUTION CODE

13. ABSTRACT (*Maximum 200 words*)

This report contains results of structural analyses performed in support of the NASA structural testing of an all-composite stitched/RFI (resin film infusion) wing stub box. McDonnell Douglas Aerospace Company designed and fabricated the wing stub box. The analyses used a global/local approach. The global model contains the entire test article. It includes the all-composite stub box, a metallic load-transition box and a metallic wing-tip extension box. The two metallic boxes are connected to the inboard and outboard ends of the composite wing stub box, respectively. The load-transition box was attached to a steel and concrete vertical reaction structure and a load was applied at the tip of the extension box to bend the wing stub box upward. The local model contains an upper cover region surrounding three stringer runouts. In that region, a large nonlinear deformation was identified by the global analyses. A more detailed mesh was used for the local model to obtain more accurate analysis results near stringer runouts. Numerous analysis results such as deformed shapes, displacements at selected locations, and strains at critical locations are included in this report.

14. SUBJECT TERMS
Stitched Composites, Resin Film Infusion, Wing Box Analysis, Finite Element Analysis, Nonlinear Analysis

15. NUMBER OF PAGES
71

16. PRICE CODE
A04

17. SECURITY CLASSIFICATION OF REPORT	18. SECURITY CLASSIFICATION OF THIS PAGE	19. SECURITY CLASSIFICATION OF ABSTRACT	20. LIMITATION OF ABSTRACT
Unclassified	Unclassified	Unclassified	Unlimited